How Blinking Affects Photon Correlations in Multichromophoric Nanoparticles

Tim Schröder,[1] Sebastian Bange,[2] Jakob Schedlbauer,[2] Florian Steiner,[1] John M. Lupton,[2] Philip Tinnefeld,[1] and Jan Vogelsang[2,]*

[1]Department Chemie and Center for NanoScience (CeNS), Ludwig-Maximilians-Universität München, Butenandtstr. 5-13, 81377 München, Germany

[2]Institut für Experimentelle und Angewandte Physik and Regensburg Center for Ultrafast Nanoscopy (RUN), Universität Regensburg, Universitätsstr. 31, 93040 Regensburg, Germany

ABSTRACT

A single chromophore can only emit a maximum of one single photon per excitation cycle. This limitation results in a phenomenon commonly referred to as photon antibunching (pAB). When multiple chromophores contribute to the fluorescence measured, the degree of pAB has been used as a metric to "count" the number of chromophores. But the fact that chromophores can switch randomly between bright and dark states, also impacts pAB and can lead to incorrect chromophore numbers being determined from pAB measurements. By both simulations and experiment, we demonstrate how pAB is affected by independent and collective chromophore blinking, enabling us to formulate universal guidelines for correct interpretation of pAB measurements. We use DNA-origami nanostructures to design multichromophoric model systems that exhibit either independent or collective chromophore blinking. Two approaches are presented that can distinguish experimentally between these two blinking mechanisms. The first one utilizes the different excitation intensity dependence on the blinking mechanisms. The second approach exploits the fact that collective blinking implies energy transfer to a quenching moiety, which is a time-dependent process. In pulsed-excitation experiments, the degree of collective blinking can therefore be altered by time gating the fluorescence photon stream, enabling us to extract the energy-transfer rate to a quencher. The ability to distinguish between different blinking mechanisms is valuable in materials science, such as for multichromophoric nanoparticles like conjugated-polymer chains, as well as in biophysics, *e.g.* for quantitative analysis of protein assemblies by counting chromophores.

KEYWORDS: single-molecule spectroscopy, photon statistics, DNA-origami structures, photophysics, quantum optics

Counting the night sky's visible stars is a formidable task, not least due to omnipresent atmospheric flickering and clouds masking the line of sight. The challenge is fundamentally limited by the ability to resolve emission from close stars, which can only be overcome by ever-larger telescopes. The same limitation exists in the nanocosm when counting fluorescent chromophores. If the chromophores cannot be resolved in space,[1–5] one turns to measuring the autocorrelation statistics of emitted photons with a Hanbury Brown and Twiss (HBT) setup as illustrated in Figure 1a.[6–9] A single chromophore can only emit a single photon per unit of time that it spends in the excited state, a trademark signature of systems as varied as organic dyes,[10–13] nitrogen vacancies in diamonds,[14,15] and single ions.[16–18] This property manifests itself as a lack of autocorrelation amplitude for zero delay time, a phenomenon which is commonly referred to as photon antibunching (pAB). Correlation statistics and pAB are well understood for single chromophores but becomes very challenging to interpret for multiple chromophores in a nanoparticle. Such systems are studied in a range of material systems that are typically not associated with single photon emission, such as 2D materials,[19] clusters of quantum dots,[20] and molecular crystals.[9,21] The degree of pAB can serve as a probe for the number of emitting units in the system, and may indicate excited-state processes such as defect emission,[22] tri- and biexciton emission,[23] and singlet-singlet-annihilation (SSA).[24–26] It is often challenging to disentangle these different contributions to pAB to truly understand the underlying photophysics of a system. Recently, multichromophoric DNA-origami structures and conjugated-polymer aggregates allowed us to demonstrate that the number of chromophores can indeed be counted, even if the dye molecules interact with each other,[27,28] *e.g.* by SSA.[24–26,29] Such chromophore counting in nanoparticles is not only of significance in the context of materials science,[9] but also plays an important role in biophysics. Many protein assemblies could, in principle, be studied quantitatively by labelling

them with fluorescent dyes and subsequently counting the chromophores. Dynamic processes such as self-association and oligomerization of proteins are prominent examples, and are crucial to the operational mechanism of many such proteins.[30–33] Nanoscale clustering of membrane proteins, for example, has emerged as a common feature, possibly initiating and amplifying signal transduction across the plasma membrane, *e.g.*, in the immune response of T cells.[34] Direct experimental access to the number of participating proteins in such a process is therefore a prerequisite for a quantitative technique to study these mechanisms.

Similar to counting twinkling stars, the problem of chromophore counting is compounded by the presence of random switching between states (blinking), typically between a state that shows fluorescence (bright) and a state that is essentially non-fluorescent (dark). Consider two identical but independently blinking chromophores that for a given irradiance each spend 10 % and 90 % of their time in the fluorescent and non-fluorescent state, respectively. Only for 1 % of the measurement time would both chromophores simultaneously reside in their fluorescent state. During 81% of the measurement time, both chromophores would simultaneously be in their dark state and would thus not contribute to the photon statistics. For the remaining 18 % of the measurement time, though, only one single dye molecule is emissive. Although two blinking dyes are present in principle, the measured fluorescence intensity autocorrelation and the pAB are then dominated by the characteristics of one single dye molecule. Obviously, this situation changes dramatically when the blinking process of the two chromophores is correlated. The occurrence of luminescence blinking and the type of blinking, *i.e.* collective or individual, must therefore be taken into consideration for the correct interpretation of the pAB signal. Unfortunately, chromophore blinking is a common process with many different physical origins, *e.g.*, the formation of triplet states,[35–37] radical states,[36,38,39] energy transfer to a nearby quencher,[40–42] or

non-radiative Auger recombination such as occurs in semiconductor nanocrystals.[43] In some cases, the blinking can be reduced by photostabilizing agents,[38,44–49] but it is almost impossible to completely turn off the blinking, especially for chromophores embedded in solid-state environments.

Here, we demonstrate how the pAB signal is affected by independent and collective chromophore blinking by using both simulations of the rate equations as well as controlled experimental model systems, allowing us to formulate universal guidelines for the correct interpretation of pAB data in any multichromophoric aggregate material system.

We make use of DNA origami to design multi-chromophoric probes, which exhibit either independent or collective blinking of the chromophores, and present two approaches to distinguish experimentally between these two blinking mechanisms. The first one utilizes different dependencies of the pAB signal on the excitation intensities with respect to the blinking mechanism. The second approach exploits the fact that collective blinking implies energy transfer to a quencher, which is a time dependent process. Therefore, the effective degree of collective blinking can be altered by time-gating the photon stream under pulsed excitation, which also enables us to extract the energy transfer rate to a quencher.

RESULTS AND DISCUSSION

The inherent challenge in counting blinking chromophores by pAB with an HBT setup is illustrated in Figure 1. Under a confocal microscope, a pulsed laser source excites a chromophore (red circle). The excited electronic system releases the stored energy by emitting at most one fluorescence photon per excitation pulse and chromophore. A 50/50 beam splitter distributes the fluorescence photons on two photodetectors, and a time correlated single photon counting

(TCSPC) system records the events detected. This allows calculation of the normalized second-order intensity correlation.[50,51]

$$g^{(2)}(\Delta\tau) = \frac{\langle I_1(t)\cdot I_2(t+\Delta\tau)\rangle}{\langle I_1(t)\rangle\langle I_2(t)\rangle} \qquad \text{eq. 1}$$

which correlates the intensity measured on one detector with the intensity measured on the other one as a function of the lag time $\Delta\tau$.

This correlation is shown on the left ordinate in Figure 1b. On the other hand, one can also simply count the number of correlation events, N, *i.e.* the simultaneously detected photon events on both detectors as a function of lag time $\Delta\tau$. This approach is indicated on the right ordinate in Figure 1b, binned in integral multiples of the excitation pulse repetition time. There are essentially two ways that the degree of pAB has been defined in the past - either by the ratio of central correlation events, N_c, to the average of lateral correlation events, N_ℓ, as indicated in Figure 1b; or by the value of $g^{(2)}(\Delta\tau)$ for $\Delta\tau = 0$. The N_ℓ value commonly does not include values past ± 3 laser pulse periods, or ± 37.5 ns at a repetition rate of 80 Mhz. In a system carrying n chromophores, the number of correlation events for $\Delta\tau = 0$, *i.e.* N_c, is given by $n \cdot (n-1)$, because the first photon can be emitted by n chromophores and the second photon only by the remaining $n-1$ chromophores. On the other hand, the number of correlation events for $\Delta\tau \neq 0$, *i.e.* N_ℓ, is given by n^2, because also the second photon can be emitted by n chromophores in the next excitation cycle. Therefore, N_c/N_ℓ equals $n \cdot (n-1)/n^2 = (n-1)/n$. In an ideal system, where chromophores do not undergo dark-state formation or SSA, the number of chromophores, n, can therefore be calculated from $n = (1 - N_c/N_\ell)^{-1}$, which also agrees to $n = \left(1 - g^{(2)}(0)\right)^{-1}$ with $g^{(2)}(0) = N_c/N_\ell$,[7] essentially corresponding to using two different normalization methods for the intensity autocorrelation.

For a single chromophore, both N_c/N_ℓ and $g^{(2)}(0)$ are zero. For two and three non-blinking chromophores these values are 0.50 and 0.67, respectively, as shown in Figure 1b. For ideal non-blinking chromophores, both equations result in the correct number of chromophores n. Figure 1c shows the correlation analysis for two simulated, non-blinking chromophores (see Supporting Information for details). Both normalizations, $g^{(2)}(0)$ and N_c/N_ℓ, yield a value of 0.5, which matches the expectation for two chromophores. In experiments, however, chromophores do not only transition between the electronic ground and first excited state. Through quantum jumps from the singlet to the triplet state, which has an excited state lifetime many orders of magnitude longer,[35,36] the otherwise continuous emission of photons, *i.e.* cycling between electronic ground and excited states, is interrupted, which causes blinking. Blinking fluorescence trajectories lead to $g^{(2)}(\Delta\tau)$ values larger than 1 (bunching) if $\Delta\tau$ falls within the range of the lifetimes of bright and dark states. Effectively, the bunching behavior stems from the fact that the photon stream, which originates from the transitions while the dye is in its singlet manifold, is interrupted for the time scale of the lifetime of the dark state. For this reason, the photons appear to be bunched provided that the molecule actually fluoresces.

Figure 1d shows $g^{(2)}(\Delta\tau)$ for the simulated emission of two equal and independent chromophores that blink stochastically. Here, we must consider three cases. First, a case where both chromophores are in the bright state. Second, a case where only one chromophore is in the bright state; and third, a case where both are in the dark state. The photon bunching associated with the emission intermittency causes $g^{(2)}(\Delta\tau)$ values of 1.5 in the range of $\Delta\tau$ values from which N_ℓ is calculated. The calculated degree of pAB is now quite different for the two metrics $g^{(2)}(0)$ and N_c/N_ℓ. The value of 0.5 expected for two chromophores is only retrieved from $g^{(2)}(0)$, whereas N_c/N_ℓ is reduced to 0.33, which would normally be associated with an effective value of

$n = 1.5$ chromophores, which, of course, is unphysical. The normalization to N_ℓ effectively averages over the two cases where either only one or both chromophores are in the bright state. On the other hand, only situations where both chromophores are in the bright state contribute to central-bin photon correlation events N_c.

Next, we consider collective blinking of two chromophores in Figure 1e. Correlated blinking is expected multichromophoric aggregates such as conjugated polymers or light-harvesting complexes,[52–55] in which, for example, a triplet exciton can annihilate multiple singlet excitons.[56–59] In this case, the degree of pAB based on the correlation events in central and lateral bins now yields the correct value of $N_c/N_\ell = 0.5$ expected for two chromophores, while $g^{(2)}(0) = 1$, which would instead correspond to an infinite number of chromophores. Obviously, $g^{(2)}(0)$ underestimates the degree of pAB for the correlated system since it averages over the emitting and the non-emitting states and thus scales linearly with the bunching amplitude. In extreme cases, even values above 1 are possible, which is usually the characteristic of thermal or chaotic light emission.

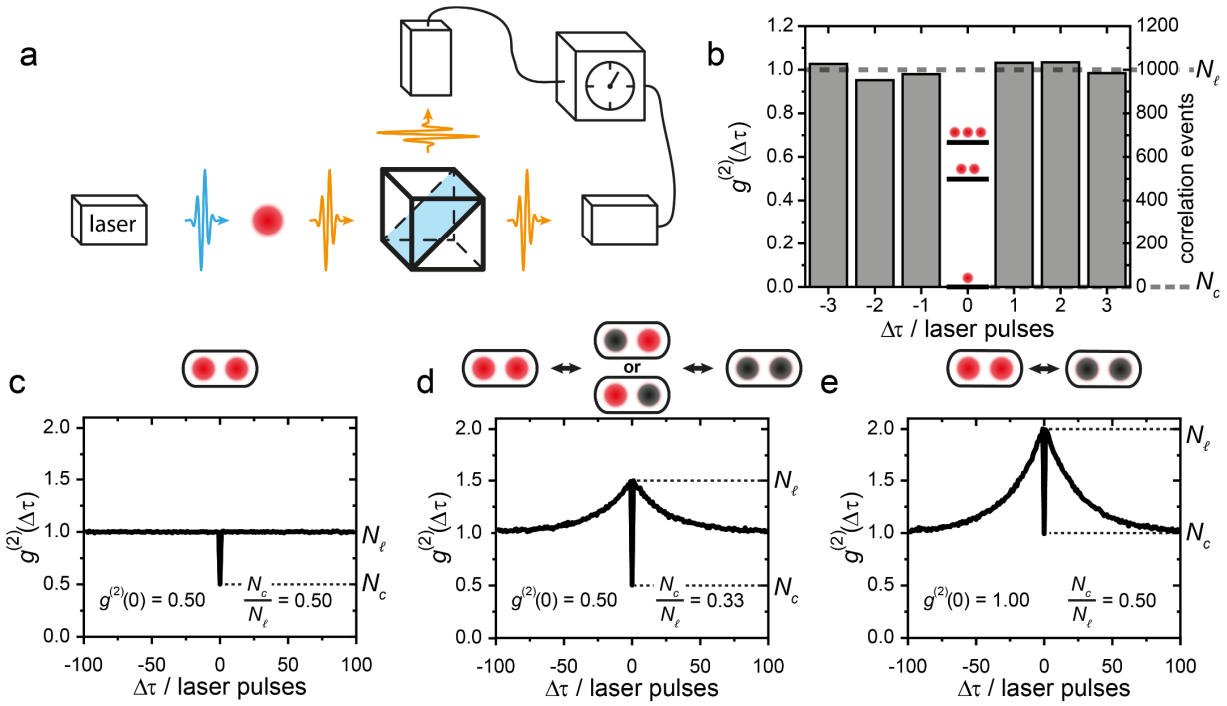

Figure 1. (a) Schematic representation of the experimental setup. A pulsed laser (blue) excites a single chromophore (red circle). The fluorescence (orange) is collected and detected in a HBT photon correlator with a 50/50 beam splitter, two single-photon detectors and a time correlator. (b) Correlation histogram with the second order intensity correlation $g^{(2)}(\Delta\tau)$ on the left ordinate and the total correlation events N on the right ordinate, respectively. The height of the central correlation count N_c reflects the number of chromophores on a reciprocal scale, examples of which are indicated by red dots. (c) Correlation histogram for two simulated, ideal chromophores without any dark states. (d) Correlation histogram for two simulated, independently blinking chromophores. The blinking results in photon bunching in the correlation histogram, while $g^{(2)}(0)$ yields the correct number of chromophores. (e) Correlation histogram for two simulated, collectively blinking chromophores. For this blinking behavior, N_c/N_ℓ yields the correct number of chromophores but not $g^{(2)}(0)$.

Although it is straightforward to simulate both independently and collectively blinking quantum systems, the effect of the different blinking mechanisms has not previously been demonstrated experimentally. As a model system for independently blinking chromophores, we positioned two ATTO 647N dye molecules in a DNA origami structure, which provides us with precise control over the distance between the two dyes as well as their immediate environment.[60–62] A dye separation of 12 nm was chosen to minimize any mutual interaction. Both chromophores were excited with a pulsed laser at a wavelength of 640 nm with a repetition rate of 40 MHz. To minimize photobleaching over time, we used an enzymatic oxygen scavenger system of glycose oxidase and catalase.[49] For fast blinking kinetics, 2 mM of freshly prepared Trolox is added to the buffer.[49] With fresh Trolox, fast blinking is observed due to the formation of radical anions that are re-oxidized by trace amounts of Trolox-quinone, yielding off-times in the range of 10-100 ms.[49] A short section of a fluorescence time trace of such a model system at 1.1 kW/cm^2 excitation power is shown in Figure 2a (for the complete fluorescence trajectory, see Figure S4). In the intensity histogram calculated based on the full dataset and shown on the right of Figure 2a, three characteristic intensity levels at 0, 15 and 30 kHz can be identified. These correspond to either none, only one, or both dyes being in the dark state, respectively. The second-order intensity correlation $g^{(2)}(\Delta\tau)$ in Figure 2b is shown on a logarithmic time scale, which allows better appreciation of the intensity dynamics over several orders of magnitude in delay time.[63] As expected for two dye chromophores, $g^{(2)}(0)$=0.52 for this dataset. On the other hand, $N_\mathrm{c}/N_\ell = 0.36$, a value much lower than expected. This value is artificially lowered because the intensity level with only one chromophore being in the bright state contributes only to lateral correlation events N_ℓ but not to central correlation events N_c.

Experimental realization of collective blinking of two organic dye molecules is much more challenging.[24] The main difficulty is that collectively blinking systems exhibit weak interchromophoric coupling not only through singlet-dark-state annihilation (SDA), but also due to SSA. Such processes all depend on energy transfer efficiency, which is governed by the spectral and photophysical properties of the dyes involved.[24] This significantly reduces the chance of detecting photon pairs and lowers the apparent number of chromophores.[24–27,64,65] SSA therefore usually tends to counteract the apparent increase of $g^{(2)}(0)$ in systems with collective blinking. In order to study the role of collective blinking, reliable and well-controlled model systems are thus needed, which at the same time show both strong SDA and negligible levels of SSA. To this end, dye molecules need to be separated by a distance at which the effect of SSA can be neglected. On the other hand, the weak chromophore-chromophore coupling necessary for SDA and collective blinking to occur needs to be retained. We overcome this problem by placing a switchable Förster Resonance Energy Transfer (FRET)-absorber between two ATTO 647N dyes that are separated by 6 nm, enough to reliably suppress SSA.[40] The FRET-switch is a 1,4-oxazine dye, ATTO 700 with an excited-state lifetime of ~1.6 ns. In its singlet state, it acts as an energy sink and quenches both ATTO 647N dyes equally. The quencher or acceptor dye ATTO 700 is placed in the center of both donor dyes ATTO 647N, and therefore the FRET rate of the donor dyes to the acceptor is approximately equal. We note that this equality might not be valid if the acceptor dye is already in an excited state due to absorption of the energy of one donor dye. But even in this case, the quencher is capable of absorbing energy by transitioning to higher excited states S_n, *i.e.* singlet-singlet annihilation occurs. However, the fluorescence lifetime of the acceptor dye is very short with 1.6 ns compared to the donor dyes with 4.3 ns. For this reason, it is unlikely that the acceptor is still in its excited S_1 state once energy transfer occurs from the second donor dye. The acceptor

dye will rather relax quickly and can absorb the energy of the remaining donor dye, through ground-state absorption. This is also a very rare process because we are working in an excitation regime in which two excited donor dyes are a very rare event (an estimation of the occurrence frequency is given in the Supporting Information). What we mean here by collective blinking is that, if the acceptor dye ATTO 700 is in its ground state S_0, it will absorb the excitation energy by FRET from both donor dyes and therefore quenches both donor dyes simultaneously. Once the acceptor dye is reduced, it is not capable of absorbing energy any longer so that both donor dyes fluoresce simultaneously. We note that the orientation in space and the differences in excitation efficiency of the chromophores is not an issue in our model system because the dyes are linked by a C_6-linker to the DNA origami structure. Therefore, the dyes are free to rotate and the energy transfer process averages over all possible orientations of both donor and acceptor chromophores. However, in real systems, such as in conjugated polymer nanoparticles, the orientation of chromophores is fixed in space and plays a significant role regarding the energy transfer dynamics as discussed in ref. 27. The fluorescence of ATTO 700 can be spectrally separated from the ATTO 647N emission and will thus not contribute to the measured photon statistics. By chemically reducing the ATTO 700 dye, its absorption spectrum shifts to the blue, resulting in less quenching of the ATTO 647N dyes due to the reduced spectral overlap. A subsequent oxidation reaction recovers the ground state and the concomitant quenching action on ATTO 647N. In our experiment, a reducing and oxidizing buffer (ROXS) of Trolox and Troloxquinone switches the ATTO 700 oxidation state stochastically.[40] A section of the resulting ATTO 647N fluorescence intensity time trace at 1.1 kW/cm^2 excitation power is shown in Figure 2c. Here, only two intensity states are clearly visible, both in the time trace as well as in the corresponding intensity histogram (the complete fluorescence time trace is shown in Figure S5). The intensity correlation in Figure

2d shows the expected photon bunching on a time scale of tens of milliseconds. For this data set, $g^{(2)}(0) = 0.87$ is indeed much larger than the expected value of 0.5. The resulting apparent number of $n \approx 7 - 8$ chromophores obviously overestimates the actual number of chromophores, because it scales with the photon bunching amplitude as discussed above. In contrast, $N_c/N_\ell = 0.51$ yields the correct degree of pAB.

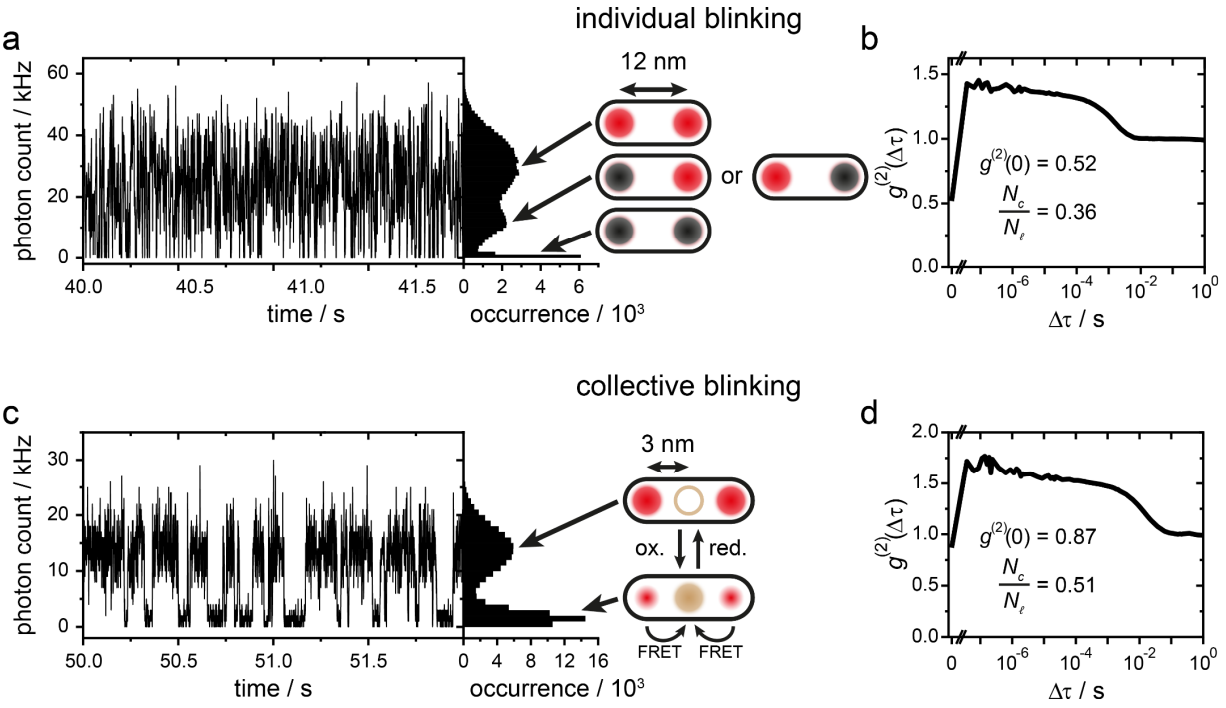

Figure 2. (a) A short section of a representative fluorescence time trace of two independently blinking ATTO 647N dyes with 12 nm spacing at 1.1 kW/cm^2 excitation power. The intensity histogram on the right side is based on the full trajectory covering 38 s of measurement time and shows three characteristic intensity levels at 0, 15 and 30 kHz. (b) Corresponding second-order intensity correlation on a logarithmic delay-time scale. In this case, $g^{(2)}(0)$ yields the correct value for two dyes. (c) A short section of a representative fluorescence time trace of two collectively blinking ATTO 647N dyes, controlled by an intermediate ATTO 700 FRET-switch, measured at

1.1 kW/cm^2 excitation power. The separation between the two ATTO 647N dyes is ~6 nm to minimize SSA, while at the same time allowing for sufficient quenching by the ATTO 700 dye. The intensity histogram on the right is based on the full intensity trajectory covering 110 s of measurement time and shows only two intensity levels. (d) Second-order intensity correlation corresponding to the fluorescence time trace of (c) on a logarithmic delay-time scale. Here, N_c/N_ℓ instead yields the correct value for two dyes.

As we have demonstrated so far, the applicability of the degree of pAB as measured by either N_c/N_ℓ or $g^{(2)}(0)$ for chromophore counting is strongly influenced by the switching dynamics between bright and dark states and the associated contributions to photon bunching. While the average time that a chromophore stays in the dark state is constant in our experiments, the time for switching into the dark state shortens with rising excitation power as was demonstrated before and in the Supporting Information for the fluorescence transient of Figure S4 for the dyes used here.[56,66] Figure 3 shows histograms for the degree of pAB for the two-chromophore model systems at excitation powers of 1.1 kW/cm^2 and 4.3 kW/cm^2. We note that the fluorescence signal increases linearly from ~15 kHz up to ~58.5 kHz for excitation powers of 1.1 and 4.3 kW/cm², respectively, which means that we are in a linear excitation regime where SSA and multiphoton processes with photophysical pathways involving higher excited states can be neglected.[67] Figure 3a and 3b show results for $g^{(2)}(0)$ and N_c/N_ℓ, respectively, for the system with independently blinking chromophores. A total of 89 dye-labeled DNA-origami structures was measured. Only DNA origami structures were measured on which all dyes were attached. Even though the dyes are very photostable under ROXS stabilization, photobleaching or spectral shifts will occur eventually during the measurement and impact the photon statistics. Therefore, we analyzed the individual transients until a bleaching event occurs or a significant spectral shift was observed as

demonstrated in the Supporting Information Figures S4-S6. For both excitation intensities, similar Gaussian $g^{(2)}(0)$ distributions with mean values of 0.483 ± 0.006 at 1.1 kW/cm^2 and 0.493 ± 0.007 at 4.3 kW/cm^2 are found, close to the expected value of 0.5 for two chromophores. On the other hand, the histograms for N_c/N_ℓ in Figure 3b show a systematic shift towards lower values for the higher excitation intensity, as the photon bunching amplitude is suppressed. We obtain average values of 0.333 ± 0.006 for 1.1 kW/cm^2 and 0.221 ± 0.007 at 4.3 kW/cm^2. These results can again be rationalized by the sensitivity of the N_ℓ measurement to cases where only one chromophore is in the dark state. These cases do not contribute to the value of N_c.

Figure 3c and 3d show histograms for $g^{(2)}(0)$ and N_c/N_ℓ values determined for 87 different measurements of collectively blinking single DNA-origami structures using the same set of excitation powers. The blinking kinetics of ATTO 700 attached to the DNA origami is less uniform compared to the case of independent blinking, so that the histograms appear broader than those in Figure 3a and b. The calculated mean values for $g^{(2)}(0)$ are therefore systematically shifted towards higher numbers. For the $g^{(2)}(0)$ histograms in Figure 3c, the mean values are 0.82 ± 0.02 at 1.1 kW/cm² and 0.63 ± 0.01 at 4.3 kW/cm^2, corresponding to apparent numbers of chromophores n of 5.5 and 2.7, respectively. In this experiment, the amplitude scales inversely proportionally to the excitation intensity. The acceptor dye switches faster into its reduced state at higher excitation power, deactivating the quenching effect.[40] The shift back to its neutral ground state though depends on the buffer conditions, which are kept constant in the experiment. The ATTO 647N dyes therefore spend less time in the quenched state at higher excitation intensities, causing lower photon correlation amplitudes. Both N_c and N_ℓ are equally sensitive to this effect since both chromophores are either in their bright or dark state, and the N_c/N_ℓ values are nominally unaffected by changes in excitation power. The N_c/N_ℓ histograms extracted from the 87

measurements show overlapping Gaussian distributions with a mean of 0.432 ± 0.008 for 1.1 kW/cm^2 and 0.411 ± 0.007 for 4.3 kW/cm^2 excitation intensity, slightly below the value of 0.5 expected for two chromophores. This observation indicates that the two ATTO 647N dyes are not entirely independent of each other after all, but may be subject to weak SSA.

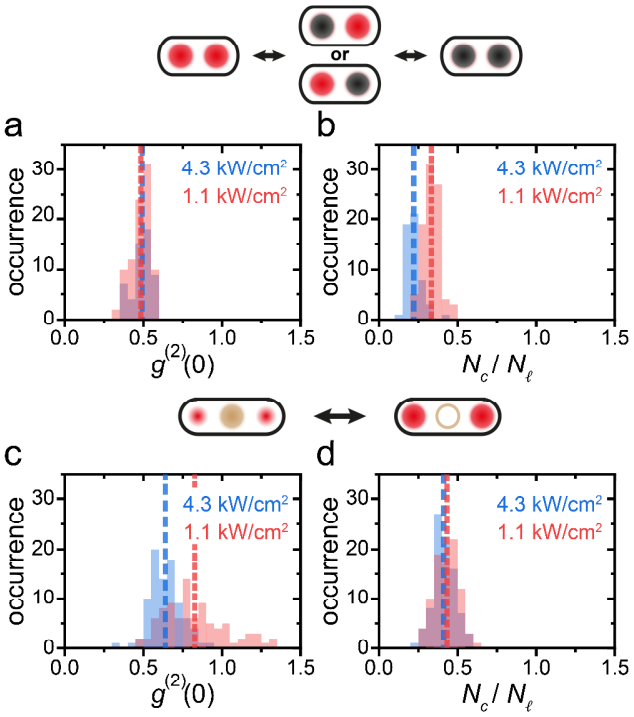

Figure 3. (a) Histogram of $g^{(2)}(0)$ values for 87 single DNA-origami particles with two independently blinking ATTO 647N dyes at excitation powers of 1.1 kW/cm^2 (red) and 4.3 kW/cm^2 (blue). The distributions have mean values of 0.483 ± 0.006 and 0.493 ± 0.007. (b) Corresponding histograms of N_c/N_ℓ values of two independently blinking ATTO 647N dyes. The mean values are 0.333 ± 0.006 and 0.221 ± 0.007. (c) Histogram of $g^{(2)}(0)$ values for 87 measured particles of two collectively blinking ATTO 647N dyes. The mean values are 0.82 ± 0.02 and 0.63 ± 0.01. (d) Corresponding N_c/N_ℓ values of two independently blinking ATTO 647N dyes with mean values of 0.432 ± 0.008 and 0.411 ± 0.007.

So far, we have only demonstrated the effect of different blinking characteristics on the photon statistics using well-defined model systems, in which energy transfer processes between the dyes can be largely neglected. In more realistic multichromophoric nanoparticles (mcNPs), however, one must consider the interplay between SSA and SDA (see Supporting Information Figure S6). For this reason, we introduce a second method to distinguish between independently and collectively blinking dyes. In mcNPs with efficient inter-chromophoric energy transfer, spontaneous triplet exciton formation on one chromophore can lead to efficient singlet-triplet annihilation (STA) for the others,[24,41,56] causing collective blinking. The observed fluorescence lifetime is then shortened, resulting in a lower fluorescence quantum yield and weaker fluorescence intensity. The fluorescence decay in this case is not monoexponential anymore because the emission switches between states with and without the presence of the triplet exciton. In contrast, the fluorescence decay of mcNPs with independently blinking dyes, *i.e.* without STA, shows a monoexponential time dependence, as triplet exciton formation on one chromophore does not affect the others. This stark difference in the fluorescence decay behavior can be exploited by microtime gating following pulsed excitation, *i.e.*, by selecting subpopulations of fluorescence photons with increasing arrival times after excitation,[68–70] and calculating $g^{(2)}(\Delta\tau)$ for each subpopulation.

The correlation amplitude depends on the contrast between the two emission intensity states.[50,51,57,69] For the case of independently blinking chromophores, we neither expect a change of the correlation amplitude nor of the photon antibunching for the different gate times, simply because the intensity contrast between the states does not change as a function of time after excitation. This is different for collectively blinking chromophores. The contrast between the two states increases from early to late microtime gates because the fluorescence of the quenched state

decays faster than the fluorescence of the unquenched state. The result is a larger intensity contrast for later microtime gates. In the following, we demonstrate this with numerical simulations (see Supporting Information for details). In Figure 4a, we simulated collective blinking for a two-chromophore system with a FRET-switch, modeled to mimic the experimental situation. As expected, the fluorescence decay is biexponential. If we consider all emitted photons (indicated by the blue area), both emission intensity states contribute to $g^{(2)}(\Delta\tau)$, shown in Figure 4d. The correlation data shows a limited amount of photon bunching, and only N_c/N_ℓ corresponds to the correct value for a two-chromophore system. Experimentally, one would not be able to decide at this point whether to use N_c/N_ℓ or $g^{(2)}(0)$ for counting the chromophores, because the underlying blinking mechanism is unknown. If photons emitted at later times (>1 ns) are considered, however, as in Figure 4b, it becomes more likely that energy transfer and SDA take place, which reduces the donor fluorescence intensity. The result is an increased intensity contrast between the bright and dark fluorescence states that leads to a higher photon correlation amplitude, shown in Figure 4e. $g^{(2)}(0)$ indicates an apparent number of 6-7 chromophores while N_c/N_ℓ stays constant and corresponds to two chromophores. Finally, we correlate only the latest arriving photons (> 3 ns), for which we do not expect to see fluorescence from the quenched state. The correlation amplitude is maximized here and only depends on the ratio of the reducing rate and the oxidizing rate of the FRET-switch. $g^{(2)}(0)$ in Figure 4f evidently scales with the amplitude and even leads to a value that one would expect for an infinite number of chromophores, whereas N_c/N_ℓ still indicates two chromophores with a value of $N_c/N_\ell = 0.50$.

Finally, we apply this microtime gating analysis to our experimental data. To perform a second-order intensity correlation with acceptable photon statistics even for the smallest time differences $\Delta\tau$, we accumulated 35 individual datasets collected from independently blinking dyes, and 39

datasets from collectively blinking dyes. The starting point of the long-pass microtime gate was chosen to increase in steps of 20 ps for each intensity correlation. The fluorescence decay of two independently blinking ATTO 647N dye molecules in Figure 4g is monoexponential, with a fluorescence lifetime of $\tau_{\mathrm{fl}} = 4.3 \pm 0.1$ ns. The measured intensity correlations are shown in Figure 4i, with gate times indicated by color and a corresponding arrow in Figure 4g. The correlation curve and the extracted values of $g^{(2)}(0)$ and N_{c}/N_{ℓ} are independent of the chosen gate time, indicating independently blinking chromophores. Based on this observation, $g^{(2)}(0)$ must be chosen to calculate the number of chromophores. Without any gating of the photons, $g^{(2)}(0) = 0.53$, slightly larger than the value of 0.5 expected for a two-chromophore system. We attribute this discrepancy to multiple excitation cycles of one single dye molecule within the same laser pulse of duration ~80 ps.[71] Long-pass gates starting at 500 ps do not suffer from this artifact.

The fluorescence decay of two collectively blinking ATTO 647N dyes in Figure 4h is biexponential and we obtain $\tau_{\mathrm{fl},1} = 0.6 \pm 0.1$ ns and $\tau_{\mathrm{fl},2} = 2.7 \pm 0.1$ ns as fluorescence lifetimes by reconvolution fits (see Supporting Information Figure S10). The intensity correlation for each gate is shown in Figure 4j with a color gradient from early (black) to late (red) gate times. The correlation amplitude rises with gate time because the contrast between the two intensity states becomes larger as a function of time after excitation. This increase is a characteristic signature of collectively blinking chromophores when an additional non-radiative pathway is introduced due to dark-state formation in a multichromophoric system. The observed $g^{(2)}(0)$ values start out at $g^{(2)}(0) = 0.8$ for the case of all photons being detected. This value would already correspond to 5 emitting chromophores, which, of course, is an unphysical result for the given material system. The value rises further for increased gate times, with the correlation amplitude reaching $g^{(2)}(0) = 0.94$ for photons detected after 1.5 ns, which would correspond to almost 17 chromophores

emitting. The rise of $g^2(0)$ with increasing gate delay is directly linked to the SDA quenching rate, which can be extracted by plotting the correlation amplitude against the starting time of the photon gate (see Supporting Information Figure S8 for a simulation and Figure S9 for experimental data; an explanation is given in the Supporting Information). From these dynamics, the SDA rate is determined to be $k_{\mathrm{SDA}} = 1.3 \pm 0.3\ \mathrm{ns}^{-1}$. In contrast, the metric N_c/N_ℓ yields values ranging from 0.43 for the case of all photons being detected to 0.41 for photons detected after a gate delay of 1.5 ns. These values are somewhat smaller than one would expect for two chromophores, which may be to be anticipated since the dye molecules are only separated by ~6 nm: in addition to SDA, SSA can still take place and reduce the probability of detecting two photons from one excitation pulse.[27] Weak SSA is also indicated by the decreasing values of N_c/N_ℓ from early to late microtime gates.[27] Microtime gating thus allows us to clearly discern the two types of blinking, independent and collective, and provides a guideline to choosing the correct spectroscopic observable for counting chromophores. For systems with strong SSA, techniques such as psTRAB must be used with the correct normalization of the photon bunching amplitude in order to correctly estimate the number of chromophores and the SSA rate.[27,70]

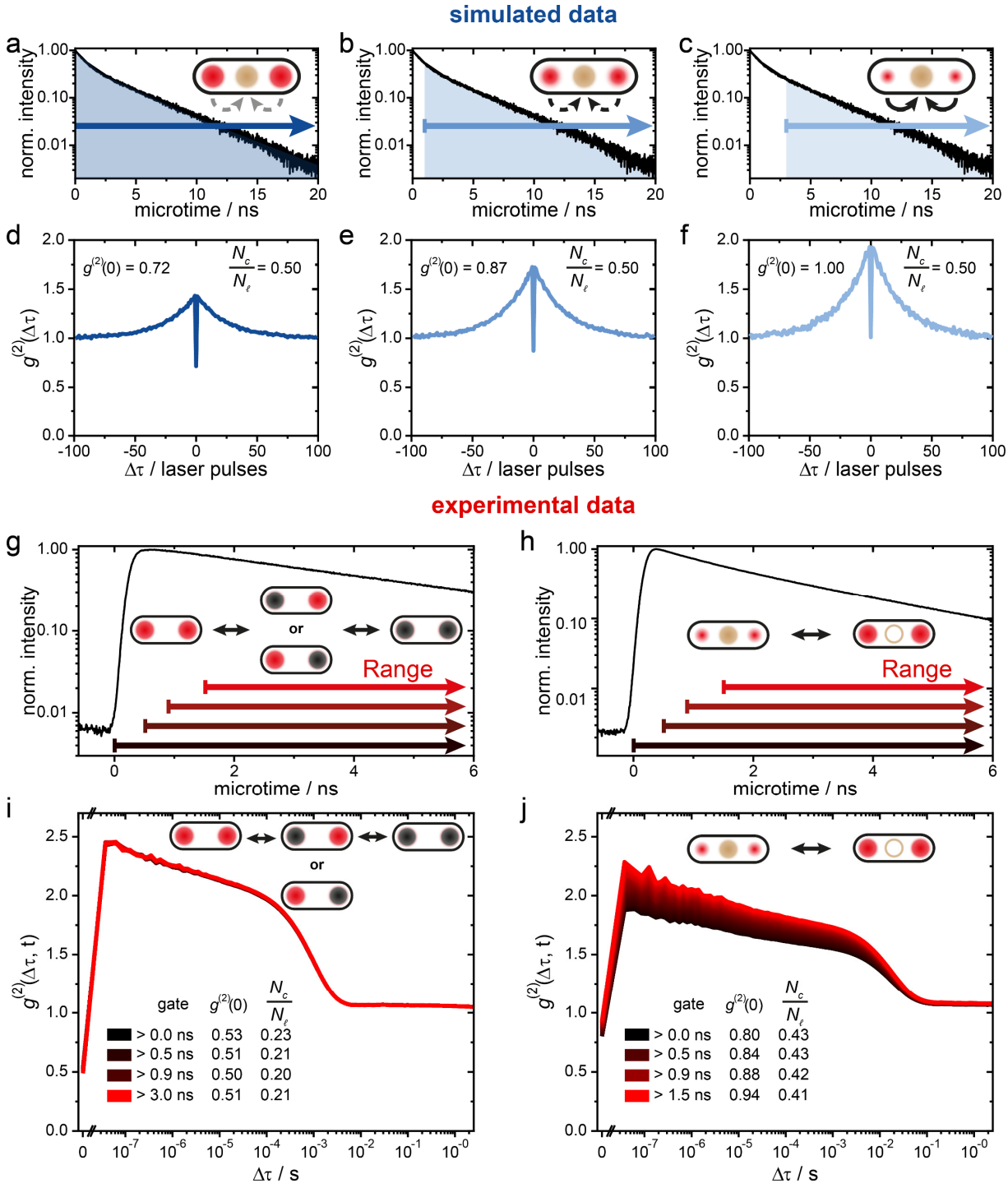

Figure 4. (a-c) Simulated fluorescence decay of two collectively blinking dye molecules showing a biexponential decay. (d-f) Corresponding second-order intensity correlation, $g^{(2)}(\Delta\tau)$, of the

long-pass gated intensity time trace. Time gates are indicated by arrows and highlighted in blue (a-c). (g) Experimental fluorescence decay of two independently blinking ATTO 647N dyes. (i) Corresponding $g^{(2)}(\Delta\tau)$ of accumulated fluorescence time traces at 4.3 kW/cm^2 excitation intensity of 35 single nanoparticles shown for four different time gates. No change of the correlation amplitude is observed with photon gating. $g^{(2)}(0)$ and N_c/N_ℓ values stay constant for different time gates, but only $g^{(2)}(0)$ yields the expected value of ~0.5. (h) Fluorescence decay of two collectively blinking ATTO 647N dye molecules. (j) Corresponding $g^{(2)}(\Delta\tau)$ of 39 compounded individual fluorescence time traces at 1.1 kW/cm^2 excitation intensity for different time gates. The correlation amplitude increases for later gate times due to the increased intensity contrast of the two luminescence intensity states. The $g^{(2)}(0)$ values scale linearly with the correlation amplitude, but only $N_c/N_\ell \approx 0.5$ reflects the expected number of chromophores considering the weak SSA occurring between the two dyes.

CONCLUSION

The issue of correct normalization of pAB measurements for blinking multichromophoric systems has mostly been neglected previously but is evidently key to counting blinking chromophores and interpreting the mutual interactions between chromophores. Different types of blinking of a multichromophoric system, *i.e.* independent or collective blinking, require very different normalizations of the pAB data. We have illustrated these challenges by both simulations and experiments. For independently blinking dyes, the normalization to lateral photon correlation events N_c/N_ℓ averages over the photon statistics due to either one or two chromophores being in the fluorescent state and thus underestimates the number of chromophores. For collectively

blinking dyes, on the other hand, the number of chromophores is instead overestimated by the normalization to the average intensity as carried out for $g^{(2)}(0)$.

We have introduced two approaches to distinguish between these two blinking mechanisms experimentally. The first approach varies the excitation power to change the blinking rate and the associated correlation amplitude. Both independent and collective blinking show inverse scaling of the correlation amplitude with excitation intensity. The second approach uses photon gating of the photon arrival times after pulsed excitation. Concomitant variation of the correlation amplitudes is characteristic for collective blinking and indicates that a N_c/N_ℓ normalization is required. However, in actual multichromophoric systems such as conjugated-polymer nanoparticles or light-harvesting complexes, both types of blinking mechanisms might occur simultaneously or change dynamically, due to the formation of a quencher. For simply counting the number of chromophores, we suggest that one should construct a second-order correlation curve only from the earliest photons after excitation, *e.g.* using a time window of ~0-400 ps after excitation, if the PL lifetime is in the range of ~4 ns as for the dyes studied here. For these photons a possible quenching process due to excitation energy transfer to a quencher within the multichromophoric aggregate can be neglected. Such energy transfer is imperative for a collective blinking process. This means that such a second-order correlation curve acquired with early time photons is dominated only by the independent blinking process, for which $g^{(2)}(0)$ must be considered to count the correct number of chromophores. On the other hand, we can also choose a time gate long after excitation, which will show a combination of both independent and collective blinking mechanisms in the second-order correlation curve. Using both correlation curves, *i.e.* for an early time window and a late-time gate, it will, in principle, be possible to also extract the quenching rate by a quencher and estimate the degree of independent and collective blinking in

the multichromophoric system. Although we refrain from discussing an experimental application here, a simulation demonstrating that $g^{(2)}(0)$ for an early time gate yields the correct number of chromophores in a system which exhibits both blinking mechanisms is given in the Supporting Information Figure S12. We note that with a HBT setup up to 8 chromophores can be counted reliably by the photon statistics,[72] but one must always ensure that PL spectra, intensity and lifetime are very similar for the individual dyes and that bleaching of the dyes is negligible. To count a higher number of chromophores by photon statistics we refer to the work of Kurz *et al.*, in which the detection scheme was extended to four detectors and a sophisticated analysis, referred to as "Counting by Photon Statistics (CoPS)", is employed.[7] These authors demonstrated that up to 36 chromophores can be counted on a DNA origami structure.[73] Our work provides a more unifying picture for the correct interpretation of photon antibunching data, resolving some possible controversies in the literature and offering a powerful tool for future analysis. After all, blinking of chromophores is the norm rather than the exception in most real physical systems.

MATERIALS AND METHODS:

Optical setup: A home-built confocal microscope based on an Olympus IX-71 inverted microscope was used for all experiments. DNA-origami structures were excited by a pulsed laser (636 nm, ~80 ps full width at half maximum, LDH-D-C-640; PicoQuant GmbH) operated at 40 MHz repetition rate. The laser power was focused to a diffraction-limited spot, with power adjusted to either 1.1 kW/cm^2 or 4.3 kW/cm^2 by means of a neutral-density filter (ND06A, Thorlabs). Circularly polarized light was obtained by a linear polarizer (LPVISE100-A, Thorlabs GmbH) and a quarter-wave plate (AQWP05M-600, Thorlabs GmbH). The light was focused onto the sample by an oil-immersion objective (UPLSAPO100XO, NA 1.40, Olympus Deutschland GmbH). The sample was moved by a piezo stage (P-517.3CD, Physik Instrumente (PI) GmbH &

Co. KG) controlled by a piezo controller (E-727.3CDA, Physik Instrumente (PI) GmbH & Co. KG). The emission was separated from the excitation beam by a dichroic beam splitter (zt532/640rpc, Chroma) and focused onto a 50 µm diameter pinhole (Thorlabs GmbH). The emission light was separated from scattered excitation light by a 647 nm long-pass filter (RazorEdge LP 647, Semrock). For collective blinking experiments, an additional 694 nm (FF02-694/SP-25, Semrock) short-pass filter was added to block the ATTO 700 emission. The filtered emission was split into two detection channels by a non-polarizing 50:50 beam splitter (CCM1-BS013/M, Thorlabs GmbH). In each detection channel, the afterglow luminescence of the avalanche photodiode was blocked by a 750 nm short-pass filter (FES0750, Thorlabs GmbH). Emission was focused onto avalanche photodiodes (SPCM-AQRH-14-TR, Excelitas Technologies GmbH & Co. KG) and the signals were registered by a multichannel picosecond event timer (HydraHarp 400, PicoQuant GmbH). The setup was controlled by a commercial software package (SymPhoTime64, Picoquant GmbH).

DNA origami structure fabrication: All DNA oligonucleotides were purchased at Eurofins Genomics Germany GmbH. The scaffold is an 8064-nucleotide-long ssDNA extracted from M13mp18 bacteriophages. Oligonucleotides modified with ATTO 542 for external labeling were purchased from biomers.net GmbH. For details of the DNA origami structures, sample preparation, and purification, see the Supporting Information. The DNA origami structures were immobilized on a LabTekTM chamber slide (Thermo Fisher Scientific Inc.) coated with BSA-biotin/neutravidin (Merck KGaA). See the protocol details in the SI.

Data acquisition and analysis: 10 µm × 10 µm scans were used to pick the DNA origami structures. The structures were measured with both 1.1 kW/cm^2 and 4.3 kW/cm^2 excitation intensity until one dye bleached. For experiments showing independently blinking dyes, a reducing

buffer system (1×TAE, 12 mM MgCl2, 2 mM Trolox (freshly prepared), 1 % (w/v) D-(+)- glucose) in combination with an oxygen scavenging system (250 U/mL glucose oxidase and 2000 U/mL catalase) was used. For collective blinking, a reducing and oxidizing buffer system (1×TAE, 12 mM $MgCl_2$, 2 mM Trolox/Troloxquinone, 1 % (w/v) D-(+)- glucose) (3) was used. The oxygen scavenging system was the same as in the independent blinking experiments. All chemicals were purchased from Merck KGaA.

Only those single-particle luminescence data sets which showed a minimum of 100 lateral-bin correlation events were analyzed to ensure an acceptable signal-to-noise ratio. The intensity correlation was performed using a self-written Python script employing the correlation algorithm introduced by Laurence *et al.*[74]

ASSOCIATED CONTENT

The Supporting Information is available free of charge at

https://pubs.acs.org/*

Supporting Information. Detailed DNA origami structures, sample preparation, details for the simulations, single-molecule intensity time traces, theory, simulation for the effect of microtime gating on the photon bunching amplitude, and simulations for simultaneous collective and individual blinking

Corresponding Author

***E-mail:** jan.vogelsang@ur.de

Author Contributions

S.B., J.M.L. and J.V. devised the methodology of the correct normalization of photon antibunching. T.S., F.S., P.T. and J.V. designed the experiment and DNA origami structures. T.S.

prepared, measured, and analyzed the DNA origami structures and data. T.S and J.S. developed the microtime-gated correlation analysis. T.S. and S.B. designed the simulations. T.S., S.B., F.S., J.M.L., P.T. and J.V. contributed to manuscript writing.

Competing financial interests

The authors declare no competing financial interests.

ACKNOWLEDGMENT

P.T., F.S. and T.S. thank the DFG under Germany´s Excellence Strategy – EXC 2089/1 – 390776260 for financial support. J.M.L. is indebted to the German Science Foundation for funding *via* grant No. 439215932 and J.V. *via* gran No. 470075523.

REFERENCES

1. Krüger, C. L.; Zeuner, M.-T.; Cottrell, G. S.; Widera, D.; Heilemann, M. Quantitative Single-Molecule Imaging of TLR4 Reveals Ligand-Specific Receptor Dimerization. *Sci. Signal.* **2017**, *10*, eaan1308.

2. Nerreter, T.; Letschert, S.; Götz, R.; Doose, S.; Danhof, S.; Einsele, H.; Sauer, M.; Hudecek, M. Super-Resolution Microscopy Reveals Ultra-Low CD19 Expression on Myeloma Cells That Triggers Elimination by CD19 CAR-T. *Nat. Commun.* **2019**, *10*, 3137.

3. Lukeš, T.; Glatzová, D.; Kvíčalová, Z.; Levet, F.; Benda, A.; Letschert, S.; Sauer, M.; Brdička, T.; Lasser, T.; Cebecauer, M. Quantifying Protein Densities on Cell Membranes Using Super-Resolution Optical Fluctuation Imaging. *Nat. Commun.* **2017**, *8*, 1731.

4. Pape, J. K.; Stephan, T.; Balzarotti, F.; Büchner, R.; Lange, F.; Riedel, D.; Jakobs, S.; Hell, S. W. Multicolor 3D MINFLUX Nanoscopy of Mitochondrial MICOS Proteins. *Proc. Natl. Acad. Sci. U.S.A.* **2020**, *117*, 20607–20614.

5. Jungmann, R.; Avendaño, M. S.; Dai, M.; Woehrstein, J. B.; Agasti, S. S.; Feiger, Z.; Rodal, A.; Yin, P. Quantitative Super-Resolution Imaging with qPAINT. *Nat. Methods* **2016**, *13*, 439–442.

6. Weston, K. D.; Dyck, M.; Tinnefeld, P.; Müller, C.; Herten, D. P.; Sauer, M. Measuring the Number of Independent Emitters in Single-Molecule Fluorescence Images and Trajectories Using Coincident Photons. *Anal. Chem.* **2002**, *74*, 5342–5349.

7. Ta, H.; Kiel, A.; Wahl, M.; Herten, D.-P. Experimental Approach to Extend the Range for Counting Fluorescent Molecules Based on Photon-Antibunching. *Phys. Chem. Chem. Phys.* **2010**, *12*, 10295–10300.

8. Grußmayer, K. S.; Herten, D.-P. Time-Resolved Molecule Counting by Photon Statistics across the Visible Spectrum. *Phys. Chem. Chem. Phys.* **2017**, *19*, 8962–8969.

9. Lupton, J. M.; Vogelsang, J. Photon Correlations Probe the Quantized Nature of Light Emission from Optoelectronic Materials. *Appl. Phys. Rev.* **2021**, *8*, 41302.

10. Lounis, B.; Moerner, W. E. Single Photons on Demand from a Single Molecule at Room Temperature. *Nature* **2000**, *407*, 491–493.

11. Fleury; Segura; Zumofen; Hecht; Wild. Nonclassical Photon Statistics in Single-Molecule Fluorescence at Room Temperature. *Phys. Rev. Lett.* **2000**, *84*, 1148–1151.

12. Ambrose, W. P.; Basché, T.; Moerner, W. E. Detection and Spectroscopy of Single Pentacene Molecules in a p-Terphenyl Crystal by Means of Fluorescence Excitation. *J. Chem. Phys.* **1991**, *95*, 7150–7163.

13. Basché, T.; Moerner, W. E.; Orrit, M.; Talon, H. Photon Antibunching in the Fluorescence of a Single Dye Molecule Trapped in a Solid. *Phys. Rev. Lett.* **1992**, *69*, 1516–1519.

14. Kurtsiefer; Mayer; Zarda; Weinfurter. Stable Solid-State Source of Single Photons. *Phys. Rev. Lett.* **2000**, *85*, 290–293.

15. Brouri, R.; Beveratos, A.; Poizat, J. P.; Grangier, P. Photon Antibunching in the Fluorescence of Individual Color Centers in Diamond. *Opt. Lett.* **2000**, *25*, 1294–1296.

16. Maunz, P.; Moehring, D. L.; Olmschenk, S.; Younge, K. C.; Matsukevich, D. N.; Monroe, C. Quantum Interference of Photon Pairs from Two Remote Trapped Atomic Ions. *Nat. Phys.* **2007**, *3*, 538–541.

17. Kolesov, R.; Xia, K.; Reuter, R.; Stöhr, R.; Zappe, A.; Meijer, J.; Hemmer, P. R.; Wrachtrup, J. Optical Detection of a Single Rare-Earth Ion in a Crystal. *Nat. Commun.* **2012**, *3*, 1029.

18. Barros, H. G.; Stute, A.; Northup, T. E.; Russo, C.; Schmidt, P. O.; Blatt, R. Deterministic Single-Photon Source from a Single Ion. *New J. Phys.* **2009**, *11*, 103004.

19. Toth, M.; Aharonovich, I. Single Photon Sources in Atomically Thin Materials. *Annu. Rev. Phys. Chem.* **2019**, *70*, 123–142.

20. Lv, B.; Zhang, H.; Wang, L.; Zhang, C.; Wang, X.; Zhang, J.; Xiao, M. Photon Antibunching in a Cluster of Giant CdSe/CdS Nanocrystals. *Nat. Commun.* **2018**, *9*, 1536.

21. Stangl, T.; Wilhelm, P.; Remmerssen, K.; Höger, S.; Vogelsang, J.; Lupton, J. M. Mesoscopic Quantum Emitters from Deterministic Aggregates of Conjugated Polymers. *Proc. Natl. Acad. Sci. U.S.A.* **2015**, *112*, E5560-6.

22. Koperski, M.; Nogajewski, K.; Arora, A.; Cherkez, V.; Mallet, P.; Veuillen, J.-Y.; Marcus, J.; Kossacki, P.; Potemski, M. Single Photon Emitters in Exfoliated WSe2 Structures. *Nat. Nanotechnol.* **2015**, *10*, 503–506.

23. Fisher, B.; Caruge, J. M.; Zehnder, D.; Bawendi, M. Room-Temperature Ordered Photon Emission from Multiexciton States in Single CdSe Core-Shell Nanocrystals. *Phys. Rev. Lett.* **2005**, *94*, 87403.

24. Hofkens, J.; Cotlet, M.; Vosch, T.; Tinnefeld, P.; Weston, K. D.; Ego, C.; Grimsdale, A.; Müllen, K.; Beljonne, D.; Brédas, J. L.; Jordens, S.; Schweitzer, G.; Sauer, M.; Schryver, F. de. Revealing Competitive Forster-Type Resonance Energy-Transfer Pathways in Single Bichromophoric Molecules. *Proc. Natl. Acad. Sci. U.S.A.* **2003**, *100*, 13146–13151.

25. Hübner, C. G.; Zumofen, G.; Renn, A.; Herrmann, A.; Müllen, K.; Basché, T. Photon Antibunching and Collective Effects in the Fluorescence of Single Bichromophoric Molecules. *Phys. Rev. Lett.* **2003**, *91*, 93903.

26. Tinnefeld, P.; Weston, K. D.; Vosch, T.; Cotlet, M.; Weil, T.; Hofkens, J.; Müllen, K.; Schryver, F. C. de; Sauer, M. Antibunching in the Emission of a Single Tetrachromophoric Dendritic System. *J. Am. Chem. Soc.* **2002**, *124*, 14310–14311.

27. Hedley, G. J.; Schröder, T.; Steiner, F.; Eder, T.; Hofmann, F. J.; Bange, S.; Laux, D.; Höger, S.; Tinnefeld, P.; Lupton, J. M.; Vogelsang, J. Picosecond Time-Resolved Photon Antibunching Measures Nanoscale Exciton Motion and the True Number of Chromophores. *Nat. Commun.* **2021**, *12*, 1327.

28. Schindler, F.; Jacob, J.; Grimsdale, A. C.; Scherf, U.; Müllen, K.; Lupton, J. M.; Feldmann, J. Counting Chromophores in Conjugated Polymers. *Angew. Chem. Int. Ed.* **2005**, *44*, 1520–1525.

29. Becker, K.; Lagoudakis, P. G.; Gaefke, G.; Höger, S.; Lupton, J. M. Exciton Accumulation in Pi-Conjugated Wires Encapsulated by Light-Harvesting Macrocycles. *Angew. Chem. Int. Ed.* **2007**, *46*, 3450–3455.

30. Matthews, J. M. *Protein Dimerization and Oligomerization in Biology* 747; Springer New York: New York, NY, 2012.

31. Havugimana, P. C.; Hart, G. T.; Nepusz, T.; Yang, H.; Turinsky, A. L.; Li, Z.; Wang, P. I.; Boutz, D. R.; Fong, V.; Phanse, S.; Babu, M.; Craig, S. A.; Hu, P.; Wan, C.; Vlasblom, J.; Dar, V.-u.-N.; Bezginov, A.; Clark, G. W.; Wu, G. C.; Wodak, S. J. *et al.* A Census of Human Soluble Protein Complexes. *Cell* **2012**, *150*, 1068–1081.

32. Ahnert, S. E.; Marsh, J. A.; Hernández, H.; Robinson, C. V.; Teichmann, S. A. Principles of Assembly Reveal a Periodic Table of Protein Complexes. *Science* **2015**, *350*, aaa2245.

33. Drew, K.; Lee, C.; Huizar, R. L.; Tu, F.; Borgeson, B.; McWhite, C. D.; Ma, Y.; Wallingford, J. B.; Marcotte, E. M. Integration of Over 9,000 Mass Spectrometry Experiments Builds a Global Map of Human Protein Complexes. *Mol. Syst. Biol.* **2017**, *13*, 932.

34. Goyette, J.; Gaus, K. Mechanisms of Protein Nanoscale Clustering. *Curr. Opin. Cell Biol.* **2017**, *44*, 86–92.

35. Basché, T.; Kummer, S.; Bräuchle, C. Direct Spectroscopic Observation of Quantum Jumps of a Single Molecule. *Nature* **1995**, *373*, 132–134.

36. Ha, T.; Tinnefeld, P. Photophysics of Fluorescent Probes for Single-Molecule Biophysics and Super-Resolution Imaging. *Annu. Rev. Phys. Chem.* **2012**, *63*, 595–617.

37. Widengren, J.; Chmyrov, A.; Eggeling, C.; Löfdahl, P.-A.; Seidel, C. A. M. Strategies to Improve Photostabilities in Ultrasensitive Fluorescence Spectroscopy. *J. Phys. Chem. A* **2007**, *111*, 429–440.

38. Vogelsang, J.; Kasper, R.; Steinhauer, C.; Person, B.; Heilemann, M.; Sauer, M.; Tinnefeld, P. A Reducing and Oxidizing System Minimizes Photobleaching and Blinking of Fluorescent Dyes. *Angew. Chem.* **2008**, *47*, 5465–5469.

39. Zondervan, R.; Kulzer, F.; Orlinskii, S. B.; Orrit, M. Photoblinking of Rhodamine 6G in Poly(vinyl Alcohol): Radical Dark State Formed through the Triplet. *J. Phys. Chem. A* **2003**, *107*, 6770–6776.

40. Vogelsang, J.; Cordes, T.; Forthmann, C.; Steinhauer, C.; Tinnefeld, P. Intrinsically Resolution Enhancing Probes for Confocal Microscopy. *Nano Lett.* **2010**, *10*, 672–679.

41. Tinnefeld, P.; Buschmann, V.; Weston, K. D.; Sauer, M. Direct Observation of Collective Blinking and Energy Transfer in a Bichromophoric System. *J. Phys. Chem. A* **2003**, *107*, 323–327.

42. Holzmeister, P.; Wünsch, B.; Gietl, A.; Tinnefeld, P. Single-Molecule Photophysics of Dark Quenchers as Non-Fluorescent FRET Acceptors. *Photochem. Photobiol. Sci.* **2014**, *13*, 853–858.

43. Efros, A. L.; Nesbitt, D. J. Origin and Control of Blinking in Quantum Dots. *Nat. Nanotechnol.* **2016**, *11*, 661–671.

44. Glembockyte, V.; Lincoln, R.; Cosa, G. Cy3 Photoprotection Mediated by Ni2+ for Extended Single-Molecule Imaging: Old Tricks for New Techniques. *J. Am. Chem. Soc.* **2015**, *137*, 1116–1122.

45. van der Velde, J. H. M.; Oelerich, J.; Huang, J.; Smit, J. H.; Aminian Jazi, A.; Galiani, S.; Kolmakov, K.; Guoridis, G.; Eggeling, C.; Herrmann, A.; Roelfes, G.; Cordes, T. A Simple and Versatile Design Concept for Fluorophore Derivatives with Intramolecular Photostabilization. *Nat. Commun.* **2016**, *7*, 10144.

46. Pati, A. K.; El Bakouri, O.; Jockusch, S.; Zhou, Z.; Altman, R. B.; Fitzgerald, G. A.; Asher, W. B.; Terry, D. S.; Borgia, A.; Holsey, M. D.; Batchelder, J. E.; Abeywickrama, C.; Huddle, B.; Rufa, D.; Javitch, J. A.; Ottosson, H.; Blanchard, S. C. Tuning the Baird Aromatic

Triplet-State Energy of Cyclooctatetraene to Maximize the Self-Healing Mechanism in Organic Fluorophores. *Proc. Natl. Acad. Sci. U.S.A.* **2020**, *117*, 24305–24315.

47. Holzmeister, P.; Gietl, A.; Tinnefeld, P. Geminate Recombination as a Photoprotection Mechanism for Fluorescent Dyes. *Angew. Chem.* **2014**, *53*, 5685–5688.

48. Gidi, Y.; Payne, L.; Glembockyte, V.; Michie, M. S.; Schnermann, M. J.; Cosa, G. Unifying Mechanism for Thiol-Induced Photoswitching and Photostability of Cyanine Dyes. *J. Am. Chem. Soc.* **2020**, *142*, 12681–12689.

49. Cordes, T.; Vogelsang, J.; Tinnefeld, P. On the Mechanism of Trolox as Antiblinking and Antibleaching Reagent. *J. Am. Chem. Soc.* **2009**, *131*, 5018–5019.

50. Orrit, M. Photon Statistics in Single Molecule Experiments. *Single Mol.* **2002**, *3*, 255–265.

51. Zumbusch; Fleury; Brown; Bernard; Orrit. Probing Individual Two-Level Systems in a Polymer by Correlation of Single Molecule Fluorescence. *Phys. Rev. Lett.* **1993**, *70*, 3584–3587.

52. Wientjes, E.; Renger, J.; Curto, A. G.; Cogdell, R.; van Hulst, N. F. Strong Antenna-Enhanced Fluorescence of a Single Light-Harvesting Complex Shows Photon Antibunching. *Nat. Commun.* **2014**, *5*, 4236.

53. Bopp, M. A.; Sytnik, A.; Howard, T. D.; Cogdell, R. J.; Hochstrasser, R. M. The Dynamics of Structural Deformations of Immobilized Single Light-Harvesting Complexes. *Proc. Natl. Acad. Sci. U.S.A.* **1999**, *96*, 11271–11276.

54. Krüger, T. P. J.; van Grondelle, R. The Role of Energy Losses in Photosynthetic Light Harvesting. *J. Phys. B: At. Mol. Opt. Phys.* **2017**, *50*, 132001.

55. Gwizdala, M.; Berera, R.; Kirilovsky, D.; van Grondelle, R.; Krüger, T. P. J. Controlling Light Harvesting with Light. *J. Am. Chem. Soc.* **2016**, *138*, 11616–11622.

56. Steiner, F.; Vogelsang, J.; Lupton, J. M. Singlet-Triplet Annihilation Limits Exciton Yield in Poly(3-Hexylthiophene). *Phys. Rev. Lett.* **2014**, *112*, 137402.

57. Yu, J.; Lammi, R.; Gesquiere, A. J.; Barbara, P. F. Singlet-Triplet and Triplet-Triplet Interactions in Conjugated Polymer Single Molecules. *J. Phys. Chem. B* **2005**, *109*, 10025–10034.

58. Bout, D. A. V.; Yip, W.-T.; Hu, D.; Fu, D.-K.; Swager, T. M.; Barbara, P. F. Discrete Intensity Jumps and Intramolecular Electronic Energy Transfer in the Spectroscopy of Single Conjugated Polymer Molecules. *Science* **1997**, *277*, 1074–1077.

59. Schedlbauer, J.; Scherf, U.; Vogelsang, J.; Lupton, J. M. Dynamic Quenching of Triplet Excitons in Single Conjugated-Polymer Chains. *J. Phys. Chem. Lett.* **2020**, *11*, 5192–5198.

60. Schmied, J. J.; Gietl, A.; Holzmeister, P.; Forthmann, C.; Steinhauer, C.; Dammeyer, T.; Tinnefeld, P. Fluorescence and Super-Resolution Standards Based on DNA Origami. *Nat. Methods* **2012**, *9*, 1133–1134.

61. Gietl, A.; Holzmeister, P.; Grohmann, D.; Tinnefeld, P. DNA Origami as Biocompatible Surface to Match Single-Molecule and Ensemble Experiments. *Nucleic Acids Res.* **2012**, *40*, e110.

62. Scheckenbach, M.; Bauer, J.; Zähringer, J.; Selbach, F.; Tinnefeld, P. DNA Origami Nanorulers and Emerging Reference Structures. *APL Mater.* **2020**, *8*, 110902.

63. Widengren, J.; Mets, Ü.; Rigler, R. Photodynamic Properties of Green Fluorescent Proteins Investigated by Fluorescence Correlation Spectroscopy. *Chem. Phys.* **1999**, *250*, 171–186.

64. Schröder, T.; Scheible, M. B.; Steiner, F.; Vogelsang, J.; Tinnefeld, P. Interchromophoric Interactions Determine the Maximum Brightness Density in DNA Origami Structures. *Nano Lett.* **2019**, *19*, 1275–1281.

65. Helmerich, D. A.; Beliu, G.; Sauer, M. Multiple-Labeled Antibodies Behave Like Single Emitters in Photoswitching Buffer. *ACS Nano* **2020**, *14*, 12629–12641.

66. Steinhauer, C.; Forthmann, C.; Vogelsang, J.; Tinnefeld, P. Superresolution Microscopy on the Basis of Engineered Dark States. *J. Am. Chem. Soc.* **2008**, *130*, 16840–16841.

67. Tinnefeld, P.; Hofkens, J.; Herten, D.-P.; Masuo, S.; Vosch, T.; Cotlet, M.; Habuchi, S.; Müllen, K.; Schryver, F. C. de; Sauer, M. Higher-Excited-State Photophysical Pathways in Multichromophoric Systems Revealed by Single-Molecule Fluorescence Spectroscopy. *ChemPhysChem* **2004**, *5*, 1786–1790.

68. Keller, R. A.; Ambrose, W. P.; Goodwin, P. M.; Jett, J. H.; Martin, J. C.; Wu, M. Single-Molecule Fluorescence Analysis in Solution. *Appl. Spectrosc.* **1996**, *50*, 12–32.

69. Lamb, D. C.; Schenk, A.; Röcker, C.; Scalfi-Happ, C.; Nienhaus, G. U. Sensitivity Enhancement in Fluorescence Correlation Spectroscopy of Multiple Species Using Time-Gated Detection. *Biophys. J.* **2000**, *79*, 1129–1138.

70. Benjamin, E.; Yallapragada, V. J.; Amgar, D.; Yang, G.; Tenne, R.; Oron, D. Temperature Dependence of Excitonic and Biexcitonic Decay Rates in Colloidal Nanoplatelets by Time-Gated Photon Correlation. *J. Phys. Chem. Lett.* **2020**, *11*, 6513–6518.

71. Schedlbauer, J.; Wilhelm, P.; Grabenhorst, L.; Federl, M. E.; Lalkens, B.; Hinderer, F.; Scherf, U.; Höger, S.; Tinnefeld, P.; Bange, S.; Vogelsang, J.; Lupton, J. M. Ultrafast Single-Molecule Fluorescence Measured by Femtosecond Double-Pulse Excitation Photon Antibunching. *Nano Lett.* **2020**, *20*, 1074–1079.

72. Masuo, S.; Vosch, T.; Cotlet, M.; Tinnefeld, P.; Habuchi, S.; Bell, T. D. M.; Oesterling, I.; Beljonne, D.; Champagne, B.; Müllen, K.; Sauer, M.; Hofkens, J.; Schryver, F. C. de. Multichromophoric Dendrimers as Single-Photon Sources: A Single-Molecule Study. *J. Phys. Chem. B* **2004**, *108*, 16686–16696.

73. Kurz, A.; Schmied, J. J.; Grußmayer, K. S.; Holzmeister, P.; Tinnefeld, P.; Herten, D.-P. Counting Fluorescent Dye Molecules on DNA Origami by Means of Photon Statistics. *Small* **2013**, *9*, 4061–4068.

74. Laurence, T. A.; Fore, S.; Huser, T. Fast, Flexible Algorithm for Calculating Photon Correlations. *Opt. Lett.* **2006**, *31*, 829–831.

Supplementary Information for

How Blinking Affects Photon Correlations in Multichromophoric Nanoparticles

Tim Schröder,[1] Sebastian Bange,[2] Jakob Schedlbauer,[2] Florian Steiner,[1] John M. Lupton,[2] Philip Tinnefeld,[1] and Jan Vogelsang[2,]*

[1]Department Chemie and Center for NanoScience (CeNS), Ludwig-Maximilians-Universität München, Butenandtstr. 5-13, 81377 München, Germany

[2]Institut für Experimentelle und Angewandte Physik, Universität Regensburg, Universitätsstrasse 31, 93040 Regensburg, Germany

KEYWORDS: single-molecule spectroscopy, photon statistics, DNA origami, photophysics, quantum optics

Details of DNA origami structures and sample preparation

The DNA origami structure was modified using caDNAno (version 0.2.2, design schematics in Fig. S1). The scaffold is an 8064-nucleotide-long ssDNA extracted from M13mp18 bacteriophages. All staple strands as well as the dye labeled oligonucleotides were purchased from Eurofins Genomics GmbH (see the end of Supplementary Information). The ATTO 542-modified oligonucleotides for external labeling were purchased from biomers.net. Scaffold and oligonucleotides were mixed according to table S1 for origami folding. The folding buffer (FB) is a Tris-EDTA buffer (1× TE, 10 mM Tris-HCl, 1 mM EDTA•Na_2) with 20 mM $MgCl_2$ and 5 mM NaCl. In the annealing process, the mixture was heated and slowly cooled down with a nonlinear thermal ramp over 16 hours according Nickels *et al.*[1] After annealing, the excess staples were removed with polyethylene glycol (PEG) precipitation. The samples were mixed with an equal volume of PEG precipitation buffer (1× TAE, 15 % (w/v) PEG-8000, 500 mM NaCl, 12 mM $MgCl_2$) and centrifuged at 16 krcf (thousand relative centrifugal force, *i.e.* 1000 *g*) for 30 min at 4 °C. After removing the supernatant, the pellet was suspended in 1× FB. Afterwards, the DNA origami was externally labeled with ATTO 542-modified oligonucleotides. A threefold excess with respect to the extended staples was used and the structure was incubated for 20 min in a wet chamber at room temperature. The DNA origami structures were purified *via* gel electrophoresis. A 1.5 % agarose gel containing a Tris base, acetic acid and EDTA buffer (0.5× TAE, 20 mM Tris-HCl, 10 mM acetic acid, 0.5 mM EDTA) and 12 mM $MgCl_2$ was used at 60 V for 2 hours in a gel box cooled in an ice-water bath. The gel was not stained to avoid staining reagent-dye interactions. On a blue-illuminated table DNA origami structures could be seen due to the numerous ATTO 542 dyes. DNA origami structures were recovered from the target band. The samples were stored at -26 °C until further use.

Folding Table

Final concentrations for DNA origami folding are given in Table S1. The meaning of the reagents is described below:

Table S1: Folding reagents with final concentrations.

Reagent	**Final concentration / nM**
scaffold	25

core staples	225
biotin staples	250
extended staples	225
dye and refill staples	225

scaffold: Single-stranded viral 8064 nt ssDNA from M13mp18.

core staples: Contains every unmodified staples of the rectangular DNA origami. The wildtype structure is given in Ref. [2].

biotin staples: Four biotin modified staples. Modifications are placed at the 3' end.

extended staples: 13 staples extended at the 3' end for external labeling. The extended sequence is: 5' TTTTCCTCTACCACCTACATCAC 3'. Sequence for the ATTO 542 oligonucleotides: 5' GTGATGTAGGTGGTAGAGGA-ATTO 542 3'

dye and refill staples: Oligonucleotides labeled with ATTO 647N or ATTO 700 at the 5' end.

DNA origami structures

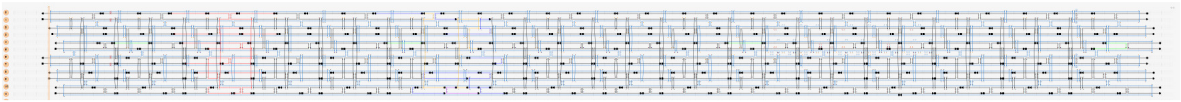

Figure S1. caDNAno sketch of the DNA origami structure used. Modified staples are colored. Green staples are biotin labeled. Red staples are extended at the 3' (5' TTTTCCTCTACCACCTACATCAC) end for external labeling with ATTO 542 modified oligonucleotides. Orange staples are labeled at the 5' end with ATTO 647N violet ones with ATTO 700. Blue staples are next to the ATTO 647N labeled staples to stabilize the structure.

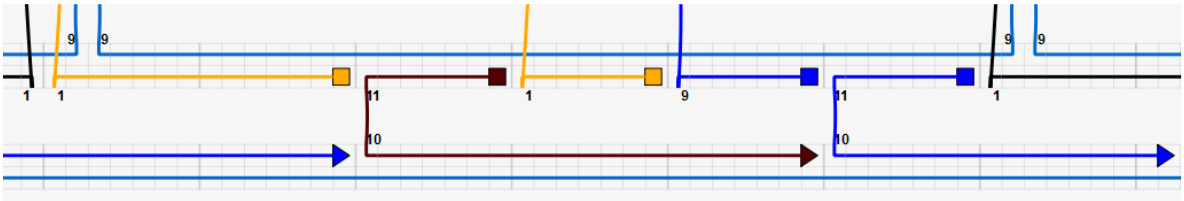

Figure S2. Close up of the DNA origami structure with two ATTO 647N (5' end of the orange staples) dyes separated by 6 nm and an ATTO 700 dye (5' end of the brown staple) for the collective blinking experiment.

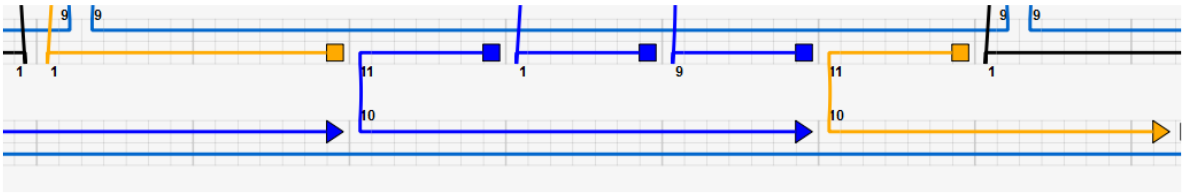

Figure S3. Close up of the DNA origami structure with two ATTO 647N (5' end of the orange staples) dyes separated by 12 nm for the independent blinking experiment.

Simulations for Figures 1 and 4

Simulations were performed with a self-written python script. The probability of detecting a photon was set to be 0.08 for intensity state A and 0.00 for intensity state B. The photons were randomly distributed on two detection channels $Ch0$ and $Ch1$. The laser repetition rate was set to be 50 MHz and 10^7 laser pulses were simulated. The simulations were analyzed based on a correlation algorithm proposed by Laurence *et al.*[3] Positive lag times correspond to the cross correlation of $Ch0 \rightarrow Ch1$ and negative lag times correspond to the correlation of $Ch1 \rightarrow Ch0$.

For blinking dyes the switching rate between state A and B was fixed to $k_A = k_B = 2 \cdot 10^6\ s^{-1}$ for each dye.

For Figure 4 the intensity levels were fixed to $I_A = 0.08$ and $I_B = 0.0016$. The fluorescence lifetime of the bright state was set to $\tau_A = 4$ ns and the fluorescence lifetime of the dark state to $\tau_B = 0.8$ ns.

Altering the correlation amplitude by excitation power for independently and collectively blinking dyes

Figure S4a shows an exemplary time trace of two independently blinking ATTO 647N dyes separated by 12 nm. With an oxygen scavenger and 2 mM Trolox as reducing agent the dyes are pushed constantly into the radical anion state. The blue and red parts of the figure correspond to an excitation power of 4.3 kW/cm^2 and 1.1 kW/cm^2, respectively. We started with the high excitation intensity. After 11 seconds, we switched to lower excitation intensity and measured until one dye bleaches at 48 s. We recorded much longer intensity time traces with lower excitation power to ensure an equal signal-to-noise ratio in the correlation calculation. The signal-to-noise ratio scales with the square of the fluorescence intensity.

Figure S4b and S4c show a two-second snapshot of the time trace in panel a, but with 1 ms binning. The intensity histogram in Figure S4b shows that most of the time, both dyes are in the non-fluorescent state for 4.3 kW/cm^2 excitation power. Figure S4c shows that at lower excitation power, the cases for one or two dyes being in their fluorescent state are more prominent.

The cross correlations for the high and low excitation power are shown in S4d with a blue and a red curve, respectively. Higher excitation powers result in higher photon bunching amplitudes for independent dyes because the bunching amplitude scales linearly with the excitation intensity. As expected for two independently blinking dyes, however, $g^{(2)}(0)$ stays constant at ~0.5 for both excitation powers. For independently blinking dyes, the ratio N_c/N_ℓ thus constitutes a pAB normalization that is inappropriate for chromophore counting.

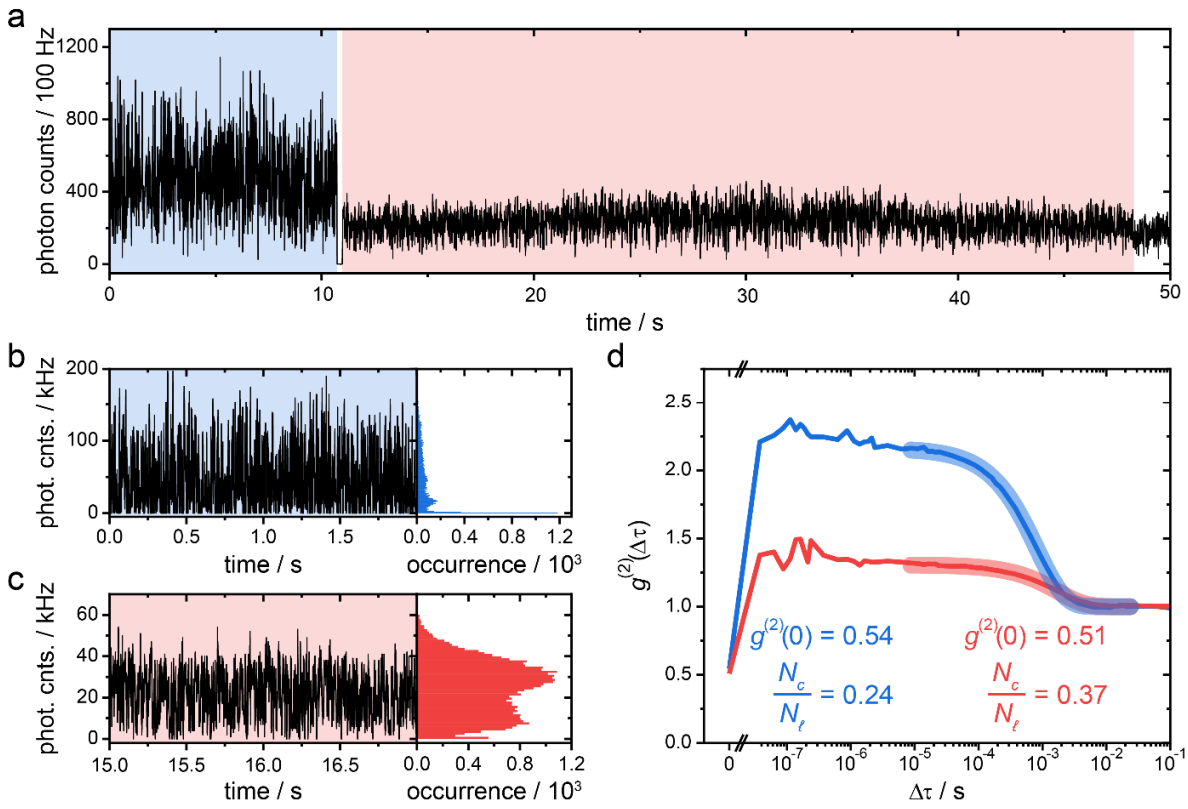

Figure S4. (a) Fluorescence time trace of two independently blinking ATTO 647N dyes separated by 12 nm. The excitation power was altered between 4.1 kW/cm^2 and 1.1 kW/cm^2 as indicated by blue and red background colors, respectively. (b) A two-second snippet of the fluorescence trajectory at 4.1 kW/cm^2 excitation with the corresponding intensity histogram. (c) A two-second snippet of the fluorescence trajectory at 1.1 kW/cm^2 excitation with corresponding intensity histogram. (d) Cross correlation of the fluorescence time trace excited with 4.1 kW/cm^2 and 1.1 kW/cm^2 shown in blue and red, respectively. Corresponding monoexponential fit from equation 9 are depicted in bold lines.

To prove that the transition rate into the singlet manifold k_{on} is power independent, we extract the transition rates from the intensity correlations shown in Figure S4d. For the extraction of the rate constants we have to consider that the observed $g^{(2)}(\Delta\tau)$ correlation is a sum of two intensity correlations each representing one independently blinking dye molecule. Since both dyes experience a similar nano-environment and excitation power, the transition rates into the dark state, k_{off}, and back again, k_{on}, are expected to be the same for both dyes, which is supported by the

monoexponential decays seen in Figure S4d. If multiple independent intensity fluctuations are involved, each correlation is weighted with the square of the fractional intensity $\mathfrak{I}$ for each dye.

$$\mathfrak{I}_1 = \frac{I_1}{\sum I_\mathrm{i}} \qquad \text{eq. 1}$$

Here, $\mathfrak{I}_1$ denotes the fractional intensity of the first dye with the measured intensity I_1. The total intensity correlation, $g^{(2)}_{\mathrm{total}}(\Delta\tau)$, can then be written as:

$$g^{(2)}_{\mathrm{total}}(\Delta\tau) = \sum \mathfrak{I}_\mathrm{i}^2 g^{(2)}_\mathrm{i}(\Delta\tau) + 1 \qquad \text{eq. 2}$$

In our case, the switching kinetics and intensities are the same for two independently blinking ATTO 647N dyes. This results in a fractional intensity of $\mathfrak{I}_1 = \mathfrak{I}_2 = \frac{1}{2}$.

$$g^{(2)}_{\mathrm{total}}(\Delta\tau) = \left(\frac{1}{2}\right)^2 g^{(2)}_1(\Delta\tau) + \left(\frac{1}{2}\right)^2 g^{(2)}_2(\Delta\tau) + 1 \quad \text{eq. 3}$$

Both dyes have the same blinking kinetics and therefore show the same intensity correlation $g^{(2)}_1(\Delta\tau) = g^{(2)}_2(\Delta\tau)$. Stochastic switching between an emitting and a non-emitting state results in a monoexponential decay in the intensity correlation.

$$g^{(2)}_{\mathrm{total}}(\Delta\tau) = \sum \mathfrak{I}_\mathrm{i}^2 \left[C_\mathrm{i} \cdot \exp\left(-k_{\mathrm{kinetics}_\mathrm{i}} \cdot \Delta\tau\right)\right] + 1 \quad \text{eq. 4}$$

For on-off-switching, the bunching amplitude C equals the equilibrium constant

$$C = K = \frac{k_\mathrm{off}}{k_\mathrm{on}} \qquad \text{eq. 5}$$

and the correlation relaxation rate k_kinetics is the sum of the switching rates

$$k_\mathrm{kinetics} = k_\mathrm{on} + k_\mathrm{off} \qquad \text{eq. 6}$$

The transition rate constants are supposed to be the same for both dyes. Therefore, they will show the same bunching amplitude $C_1 = C_2$ and the same correlation relaxation rate $k_{\mathrm{kinetics}_1} = k_{\mathrm{kinetics}_2}$. However, since both amplitudes are weighted by the square of the fractional intensity we have to consider this damping.

$$g^{(2)}_{\mathrm{total}}(\Delta\tau) = 1 + \left(\frac{1}{2}\right)^2 \left[C_1 \cdot \exp\left(-k_{\mathrm{kinetics}_1} \cdot \Delta\tau\right)\right] + \left(\frac{1}{2}\right)^2 \left[C_2 \cdot \exp\left(-k_{\mathrm{kinetics}_2} \cdot \Delta\tau\right)\right] \quad \text{eq. 8}$$

$$= 1 + \frac{1}{2} C \cdot \exp\left(-k_\mathrm{kinetics} \cdot \Delta\tau\right) \qquad \text{eq. 9}$$

With monoexponential fits using equation 9 we can extract the bunching amplitude C and correlation relaxation rate k_kinetics, which are listed for the two excitation intensities in Table S2.

Table S2: Monoexponential fit parameters from Figure S4d.

	$\boldsymbol{C}$	$\boldsymbol{k_\mathrm{kinetics}}$ **/** $\mathbf{s^{-1}}$

$\mathbf{1.1\ kW/cm^2}$	0.614 ± 0.004	581 ± 16
$\mathbf{4.1\ kW/cm^2}$	2.322 ± 0.006	1226 ± 12

With the extracted parameters we calculate the transition rates according to

$$k_{\text{on}} = \frac{k_{\text{kinetics}}}{C+1} \qquad \text{eq. 10}$$

$$k_{\text{off}} = \frac{k_{\text{kinetics}}}{\frac{1}{C}+1} \qquad \text{eq. 11}$$

The extracted rates are listed in Table S3.

Table S3: Calculated transition rate constants for two independently blinking dyes.

	$\boldsymbol{k_{\text{on}}\ /\ \text{s}^{-1}}$	$\boldsymbol{k_{\text{off}}\ /\ \text{s}^{-1}}$
$\mathbf{1.1\ kW/\ cm^2}$	359 ± 9	221 ± 5
$\mathbf{4.1\ kW/\ cm^2}$	369 ± 4	856 ± 8

The rate constant for excursions into the on-state, k_{on}, stays constant within the error for both excitation intensities, as expected. However, the transition rate into the off-state, k_{off}, is power dependent and shows a linear dependency of the excitation power. The power was raised by a factor of $\frac{4.1}{1.1} \sim 3.7$. The rate k_{off} changed by a factor of $\frac{856}{221} \sim 3.8$, which supports our statement of a linear power dependency.

A fluorescence time trace of two collectively blinking ATTO 647N dyes is shown in Figure S5a. We started with the high excitation power of 4.1 kW/cm^2 and later switched to the lower excitation power of 1.1 kW/cm^2. At 123 s, one ATTO 647N dye bleached. Figure S5b and S5c show a two-second snapshot of fluorescence trajectories with 1 ms binning. The intensity histogram shows only two intensity states for both excitation powers. The ATTO 700 FRET–switch is constantly switching between a reduced state and the singlet manifold. In the reduced state, the absorption spectrum is blue-shifted and the ATTO 647N fluorescence is not quenched. When the ATTO 700 dye is oxidized again, the ATTO 647N dyes are quenched by efficient FRET. Because we are monitoring the donor fluorescence, the bunching amplitude is inversely proportional to the excitation power. The donor dyes are stabilized by the ROXS buffer. The acceptor dye is mainly excited by FRET from the donor dyes. From its first excited energy state, it has a small chance to enter the long-living triplet state from which it can be reduced by Trolox. The time spent in the reduced state only depends on the Trolox quinone concentration and is independent of the excitation power. This fact is reflected in the intensity histograms of Figure S5b and S5c. For higher excitation power, the ATTO 647N dyes spend more time in the bright emitting state because they shelve the acceptor dye faster in the reduced state. On the other hand, with low excitation

power, the donor dyes spend more time in the quenched emitting state because it takes longer to reduce the acceptor dye.

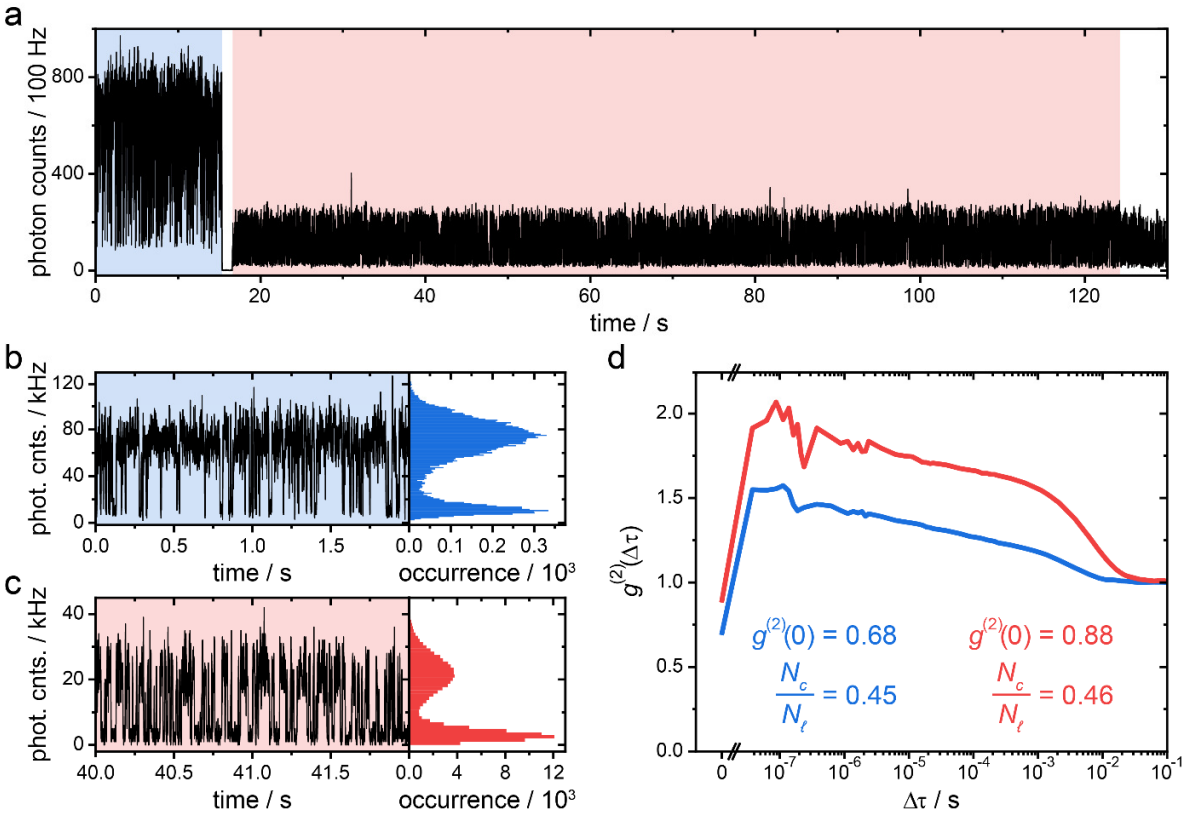

Figure S5. (a) Fluorescence time trace of two collectively blinking ATTO 647N dyes modulated by an ATTO 700 FRET-switch. The excitation power was either 4.1 kW/cm^2 (blue) or 1.1 kW/cm^2 (red). (b) Two-second snippet of the fluorescence time trace at 4.1 kW/cm^2 excitation power and the corresponding intensity histogram. (c) Two-second snippet of the fluorescence trajectory at 1.1 kW/cm^2 excitation power and the corresponding intensity histogram. (d) Cross correlation of the fluorescence time traces.

Change of excitation power does not correlate with a change in bunching amplitude

As an example of blinking kinetics which does not show a change of the correlation amplitude for different excitation powers, we chose two blinking ATTO 647N which are separated by ~3 nm, *i.e.* by 9 base pairs. The structure was published by Schröder *et al.*[4] The dyes are not independent and interact by singlet-singlet annihilation (SSA) and singlet-dark-state annihilation (SDA). To promote the dye blinking, we removed enzymatic oxygen and excited the dyes at either 1.1 kW/cm^2 and 4.1 kW/cm^2. We did not add Trolox to have sufficient singlet-triplet interactions. The fluorescence time trace for both excitation powers is shown in Figure S6a. The correlation amplitude for a single dye usually scales linearly with the excitation power. For two dyes with weak coupling this statement is not true anymore as demonstrated in Figure S6b. The correlation amplitude stays constant, but the correlation relaxation time is shifted to shorter timescales with

increasing excitation power. Due to SSA and SDA, the excitation into higher excited states becomes more likely. In higher excited states, the transition rates between the singlet and triplet state are larger and the blinking kinetics becomes faster. In our case, the rates scale with the same factor, although it varies for different dye combinations. For the antibunching measurement, we obtain $g^{(2)}(0) \sim 0.3$ and $N_c/N_\ell \sim 0.2$, which is expected for weakly collectively blinking dyes when they undergo efficient SSA.

When one dye enters the dark state, it quenches the second dye by a FRET mechanism referred to as SDA. This results in a shorter fluorescence lifetime and a quenched fluorescence signal. As described in section S5, changes of the correlation amplitude for different microtime gates shown in Figure S6c, d are a characteristic feature of collectively blinking dyes. Therefore, this correlation amplitude can be assigned to collective blinking kinetics without changing the excitation power, and the normalization of photon antibunching has to be carried out with respect to the bunching amplitude.

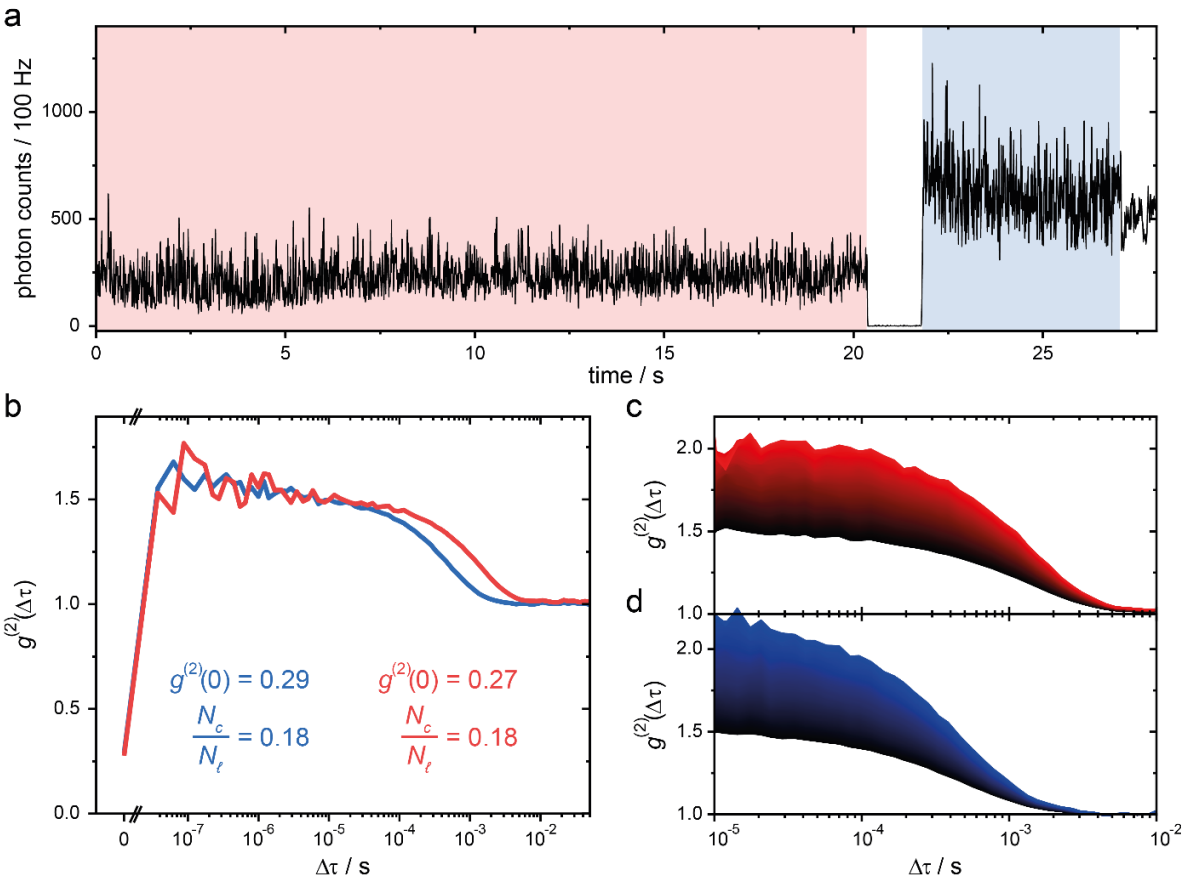

Figure S6. (a) Fluorescent trajectory of two collectively blinking ATTO 647N dyes separated by 3 nm. The excitation power was switched from 1.1 kW/cm^2 (red) to 4.1 kW/cm^2 (blue). (b) Cross-correlation of the fluorescence time traces for either excitation powers. (c) Cross-correlation for the 1.1 kW/cm^2 excitation power. The color gradient marks the beginning of the microtime gate used, which was shifted with a 20 ps step size. Black corresponds to early (from 0 ns) gate times and red to late times (up to 6 ns). (d) Cross-correlation for the 4.1 kW/cm^2 excitation power. The

color gradient marks the beginning of the microtime gate, which was shifted in 20 ps step sizes. Black corresponds to early (from 0 ns) gate times and blue to late times (up to 6 ns).

Impact of simultaneous excitation of two chromophores

The corresponding average fluorescence signals of a single chromophore are 15 kHz and 58.5 kHz, respectively, which corresponds to a linear increase for 1.1 kW/cm² and 4.3 kW/cm² excitation irradiance as shown in Figure S4. The excitation irradiance is derived by measuring the power at the back aperture of the objective, which is focused onto a diffraction-limited excitation spot. A short estimation by using the detection rate is given in the following. Two independently blinking chromophores yield, on average, a signal of 30 kHz at 1.1 kW/cm² excitation power, and by estimating a detection efficiency of 20 % this signal corresponds to 75,000 photons emitted per second per molecule. With a fluorescence quantum yield of 65 % we would excite the molecule ~115,000 times per second. The pulsed excitation rate of our laser is set to 40 MHz, which means that we excite the chromophore, on average, with every 348th pulse. If we were to have perfect singlet-singlet annihilation between two chromophores, we would lose one fluorescence photon for every 348 × 348 excitation pulses. This loss corresponds to 331 excitons per second. Taking into account the detection efficiency of the microscope, this means that ~43 photons per second are lost. The intensity would therefore drop by only 0.3 %. The same calculation yields an intensity drop of ~1.1 % for 4.3 kW/cm² excitation intensity.

Change of photon bunching with microtime gating

Random switching between two intensity states I_A and I_B is depicted in Figure S7a. The corresponding $g^{(2)}(\Delta\tau)$ intensity correlation is depicted in Figure S7b.

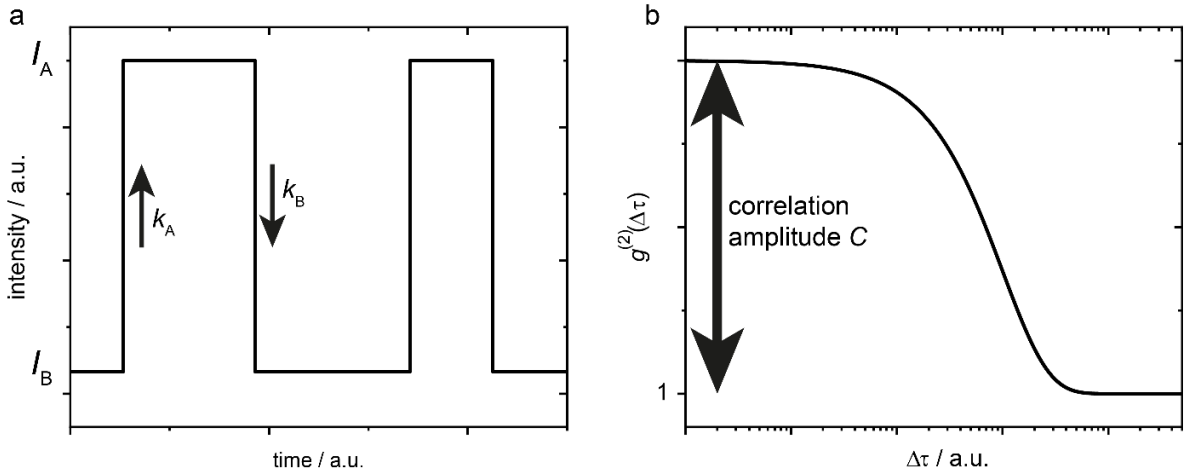

Figure S7. (a) Variation of the fluorescence intensity of a blinking molecule. (b) The corresponding correlation function on a logarithmic time scale. The correlation amplitude C is highlighted.

The correlation amplitude C of a system with two intensity states is given as:[5–8]

$$C = K\left(\frac{I_A - I_B}{I_A + K \cdot I_B}\right)^2 \qquad \text{eq. 12}$$

where I_A is the intensity of the bright fluorescent state A and I_B represents the intensity of the quenched fluorescent state B. K is the equilibrium constant calculated from the rate k_B of A → B state transitions and the rate k_A of B → A state transitions.

$$K = \frac{k_B}{k_A} \qquad \text{eq. 13}$$

The correlation amplitude C relies on the fractional intensity difference between states A and B. The quenched state B has an additional non-radiative decay from the electronic excited state. Therefore, the fluorescence decays faster after excitation in the quenched state which changes C for different microtime gates.

In our approach we vary the beginning of the microtime gate t, *i.e.* we use a long-pass time gate to change $C(t)$. We integrate over the exponential decay of the excited state from t to infinity to calculate the intensity of the quenched and unquenched state, respectively:

$$I_A(t) = \int_t^\infty e^{-(k_r + k_{nr})\cdot t'} dt' = \frac{e^{-(k_r + k_{nr})\cdot t}}{k_r + k_{nr}}, \quad \text{eq. 14}$$

$$I_B(t) = \int_t^\infty e^{-(k_r + k_{nr} + k_{SDA})\cdot t'} dt' = \frac{e^{-(k_r + k_{nr} + k_{SDA})\cdot t}}{k_r + k_{nr} + k_{SDA}}. \qquad \text{eq. 15}$$

Here, k_r and k_{nr} are the radiative and non-radiative decay rates of state A, respectively. k_{SDA} is the additional SDA rate present for state B. This leads to:

$$C(t) = K\left(\frac{\frac{e^{-(k_r + k_{nr})\cdot t}}{k_r + k_{nr}} - \frac{e^{-(k_r + k_{nr} + k_{SDA})\cdot t}}{k_r + k_{nr} + k_{SDA}}}{\frac{e^{-(k_r + k_{nr})\cdot t}}{k_r + k_{nr}} + K \cdot \frac{e^{-(k_r + k_{nr} + k_{SDA})\cdot t}}{k_r + k_{nr} + k_{SDA}}}\right)^2 = K\left(\frac{1 - \frac{k_r + k_{nr}}{k_r + k_{nr} + k_{SDA}} e^{-k_{SDA}\cdot t}}{1 + K \cdot \frac{k_r + k_{nr}}{k_r + k_{nr} + k_{SDA}} e^{-k_{SDA}\cdot t}}\right)^2 \qquad \text{eq. 16}$$

The contrast between the integrated intensities rises with the additional depletion rate k_{SDA}. Equation 16 shows that $C(t)$ depends exponentially on k_{SDA}. We assume that k_r and k_{nr} stay constant and we are only interested in the values of K and k_{SDA}. Therefore, we can rewrite eq. 5 as

$$C(t) = K\left(\frac{1 - e^{-k_{SDA}\cdot(t - t_0)}}{1 + K \cdot e^{-k_{SDA}\cdot(t - t_0)}}\right)^2, \qquad \text{eq. 17}$$

where t_0 is an artificial shift on the time axis that accounts both for the arrival time of the laser pulse and the fluorescence lifetime ratio $\frac{k_r + k_{nr}}{k_r + k_{nr} + k_{SDA}}$.

To demonstrate that this approach allows extraction of k_{SDA} from measured data, we simulated two simultaneously blinking chromophores similar to the experimental situation. The switching rates were fixed to $k_A = k_B = 10^4\ s^{-1}$ and the fluorescence lifetimes were chosen to be 4 ns for the bright and 1 ns for the quenched state. Therefore, the additional non-radiative rate for quenched state is $k_{SDA} = \frac{1}{\tau_B} - \frac{1}{\tau_A} = 0.75\ ns^{-1}$. Figure S8a shows the corresponding $g^{(2)}(\Delta\tau)$ correlation for different starting points t of the microtime gates, which were shifted in steps of 20 ps. Due to the

increasing contrast in the intensity levels, the autocorrelation amplitude rises with t. Figure S8b shows $g^{(2)}(\Delta\tau = 10^{-8}\ \mathrm{s})$ in red, which in our case is equivalent to the correlation amplitude $C(t)$ corrected by an offset of 1 for uncorrelated events. We fit the extracted value with

$$g^{(2)}(\Delta\tau = 10^{-8}\ s, t) = 1 + K\left(\frac{1-e^{-k_{\mathrm{SDA}}\cdot(t-t_0)}}{1+K\cdot e^{-k_{\mathrm{SDA}}\cdot(t-t_0)}}\right)^2 \quad \text{eq. 18}$$

The value of k_{SDA} extracted from the fit (bold semitransparent line) is $k_{\mathrm{SDA}} = 0.748 \pm 0.002\ \mathrm{ns}^{-1}$, close to the expected value of 0.75. Additionally, we plot $g^{(2)}(\Delta\tau = 0, t)$ in black, which shows a saturation towards 1 corresponding to an apparently infinite number of chromophores. The ratio of $g^{(2)}(\Delta\tau = 0, t)$ and $g^{(2)}(\Delta\tau = 3\cdot 10^{-8}\ \mathrm{s}, t)$ equals the N_c/N_ℓ ratio and stays constant at a value of 0.5, the expected value for a system with two chromophores.

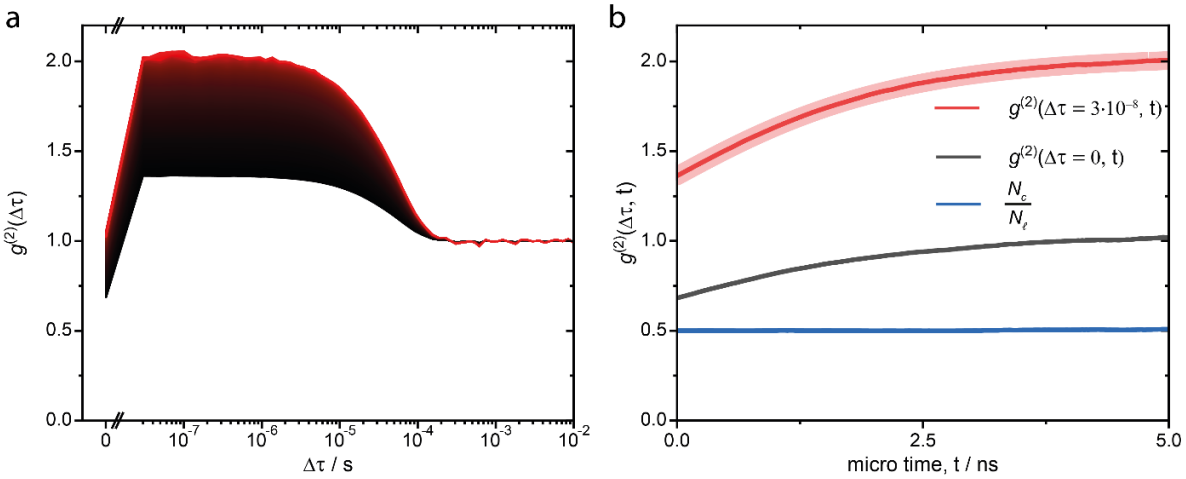

Figure S8. (a) Simulated correlation of two simultaneously blinking dyes. The color gradient marks the beginning of the microtime gate used, which was shifted with a 20 ps step size. Black corresponds to an early (from 0 ns) beginning of the microtime gate and red to a late one (up to 5 ns). (b) Extracted correlation values for $g^{(2)}(\Delta\tau = 10^{-8}\ s, t)$ (red) and $g^{(2)}(\Delta\tau = 0, t)$ (black). The red data set is fitted with eq. 7 (semitransparent bold red line). The ratio of N_c/N_ℓ is plotted in blue.

To extract the k_{SDA} rate from our experimental data we plotted the blinking amplitude of Figure 4j with a mono-exponential model to extract $C(t)$ for different beginning values of the microtime gate.

$$g^{(2)}(\Delta\tau, t) = 1 + C(t)\cdot \exp\left(-(k_{\mathrm{kinetics}})\cdot\Delta\tau\right) \quad \text{eq. 19}$$

Here, $k_{\mathrm{kinetics}} = k_{\mathrm{A}} + k_{\mathrm{B}}$ is the sum of the kinetic rates that describe the state transitions. The correlation amplitude for different microtime gates is shown in Figure S9a. The extracted correlation amplitudes $C(t)$ are plotted in Figure S9b as a black line and fitted with eq. 6. We extract k_{SDA} from the fit as $k_{\mathrm{SDA}} = 1.41 \pm 0.01\ \mathrm{ns}^{-1}$.

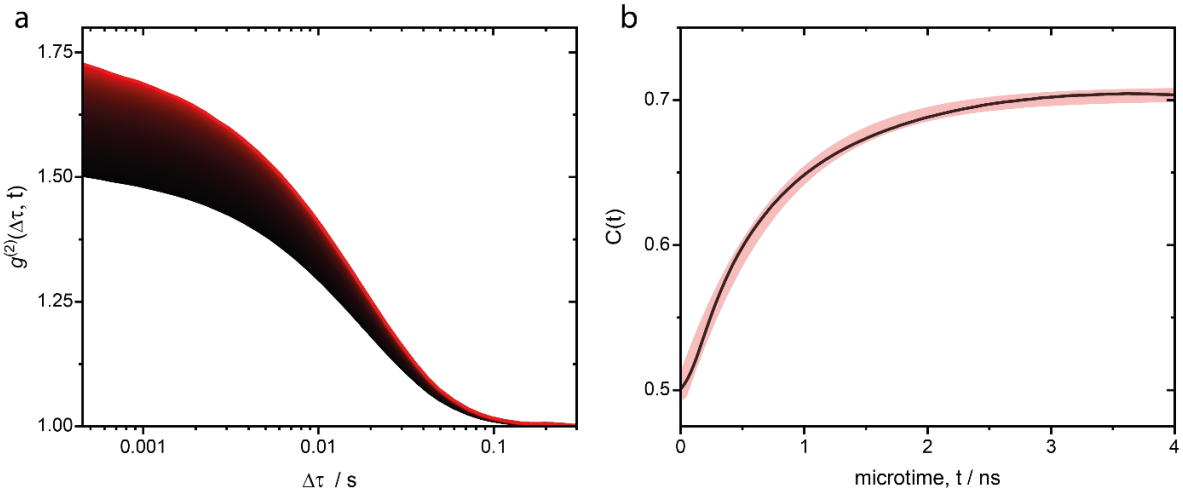

Figure S9. (a) Correlation amplitude of two collectively blinking ATTO 647N dyes. The color gradient marks the beginning of the microtime gate used, which was shifted in steps of 20 ps. Black corresponds to an early beginning (from 0 ns) of the microtime gates and red to a late (up to 4 ns) beginning. (b) Fitted correlation amplitude $C(t)$ shown in black, with a fit based on eq. 6 shown as a red semitransparent line.

Fluorescence lifetime fitting and SDA rate extraction

A reconvolution algorithm was used in order to extract the fluorescence lifetimes from the photon arrival time histograms in Figure 4g and 4h. The fluorescence lifetime decay was fitted by a convolution of the instrument response function (I_{IRF}) and the sum of fluorescence lifetime decays with amplitudes A_i, fluorescence lifetime $\tau_{\mathrm{fl},i}$ and the background intensity I_{bg}.

$$I(t) = \left(I_{\mathrm{IRF}}(t) * \sum_i A_i \cdot e^{-\frac{t-t_{\mathrm{off}}}{\tau_{\mathrm{fl},i}}} \right) + I_{\mathrm{bg}} \quad . \qquad \text{eq. 20}$$

Here, $*$ denotes the convolution operator and t_{off} represents an offset of the decay function that was introduced to compensate an intensity-dependent shift of I_{IRF}. The fit routine iterates over a range of IRF shifts and returns the fit attempt with the best reduced chi-squared test. The reconvolution fits are shown in Figure S10. The monoexponential fit model in Figure S10a works well for the independently blinking chromophore data of Figure 4i. The reduced chi squared is 1.05. A fluorescence lifetime of 4.3 $\pm$ 0.1 ns was extracted, which is expected for ATTO 647N labeled on dsDNA.[9] The monoexponential model works rather poorly for collectively blinking chrompohores as shown in Figure S10b, with a reduced chi squared of 9.72. A biexponential model is assumed to better model the presence of two intensity states of the dyes. The corresponding reconvolution fit results in reduced chi-squared values of 1.62 and the obtained lifetimes are $\tau_{\mathrm{fl},1} = 0.6 \pm 0.1$ ns and $\tau_{\mathrm{fl},2} = 2.7 \pm 0.1$ ns. The slow component shows that the ATTO 700 still absorbs slightly in its anionic radical state.

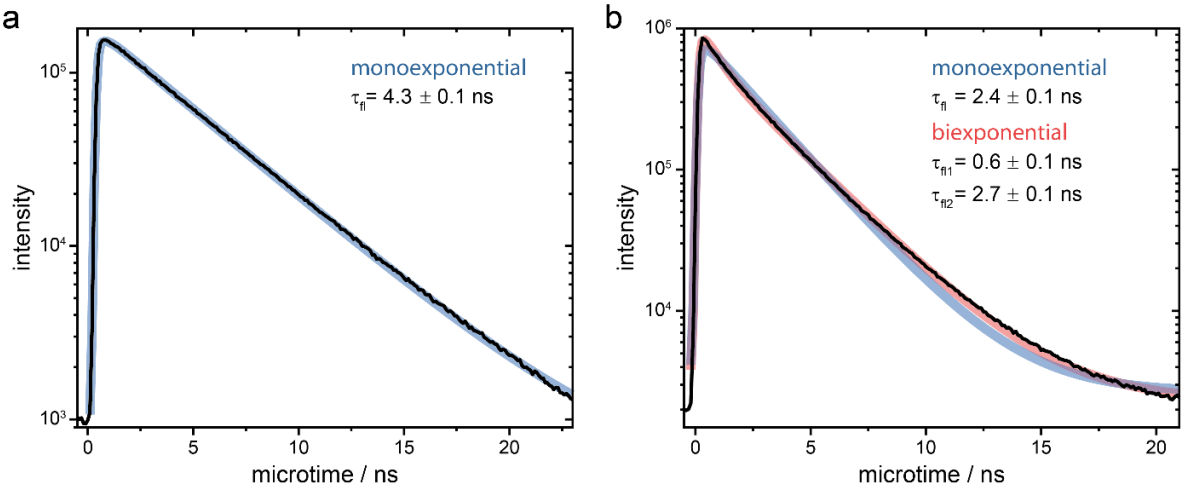

Figure S10. (a) Monoexponential reconvolution fit (blue) of the data from Figure 4g (black) with a microtime binning of 100 ps. (b) Monoexponential (blue) and biexponential (red) reconvolution fits of the data from Figure 4h (black) with a microtime binning of 100 ps.

With the fluorescence lifetimes extracted from the biexponential fit model we are able to calculate the SDA rate and validate our method as discussed in section 5.

$$\frac{1}{\tau_{\mathrm{fl},1}} - \frac{1}{\tau_{\mathrm{fl},2}} = \frac{1}{\frac{1}{k_\mathrm{r}+k_\mathrm{nr}+k_\mathrm{SDA}}} - \frac{1}{\frac{1}{k_\mathrm{r}+k_\mathrm{nr}}} = k_\mathrm{SDA} \quad \text{eq. 21}$$

This approach yields $k_\mathrm{SDA} = 1.3 \pm 0.3\ \mathrm{ns}^{-1}$, which is in good agreement with the SDA rate extracted in section 5 of $k_\mathrm{SDA} = 1.41 \pm 0.01\ \mathrm{ns}^{-1}$.

Systems with simultaneous collective and independent blinking

Multichromophoric systems could potentially show a combination of collective and independent blinking of chromophores. Both types of blinking require different normalizations of the photon antibunching measurement and therefore neither $g^{(2)}(0)$ nor N_c/N_ℓ yields the correct number of chromophores. Here, we demonstrate by simulations how a suitable subset of fluorescence photons can yield the correct value.

For the simulations we consider a simple two-chromophore system. Two chromophores are collectively quenched by an energy sink. In Figure S11, the collective switching of two chromophores into the quenched and unquenched state is denoted by the transition rate constants k_B and k_A, respectively. The independent blinking of the dyes by switching between a florescent and non-fluorescent state is denoted with k_off and the transition rate into the fluorescent state with k_on.

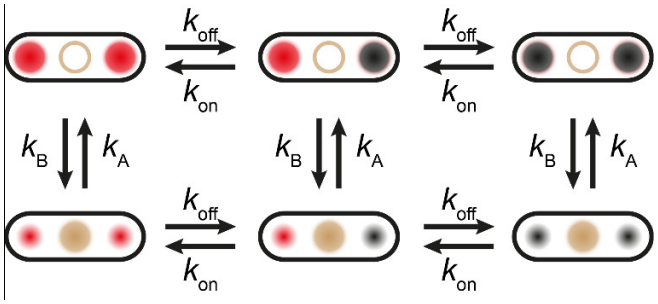

Figure S11. Sketch of all five intensity states of a system with two independently blinking dyes which can also get collectively quenched by an energy sink. We note that both states on the right are considered as one state because both states are completely non-fluorescent.

The simulations were carried out as described in Section 2. The transition rates for Figure S12a,b are set to: $k_A = k_B = 500\ s^{-1}$ and $k_{on} = k_{off} = 50\,000\ s^{-1}$. The transition rates for Figure S12c,d are set to: $k_A = k_B = 50\,000\ s^{-1}$ and $k_{on} = k_{off} = 500\ s^{-1}$.

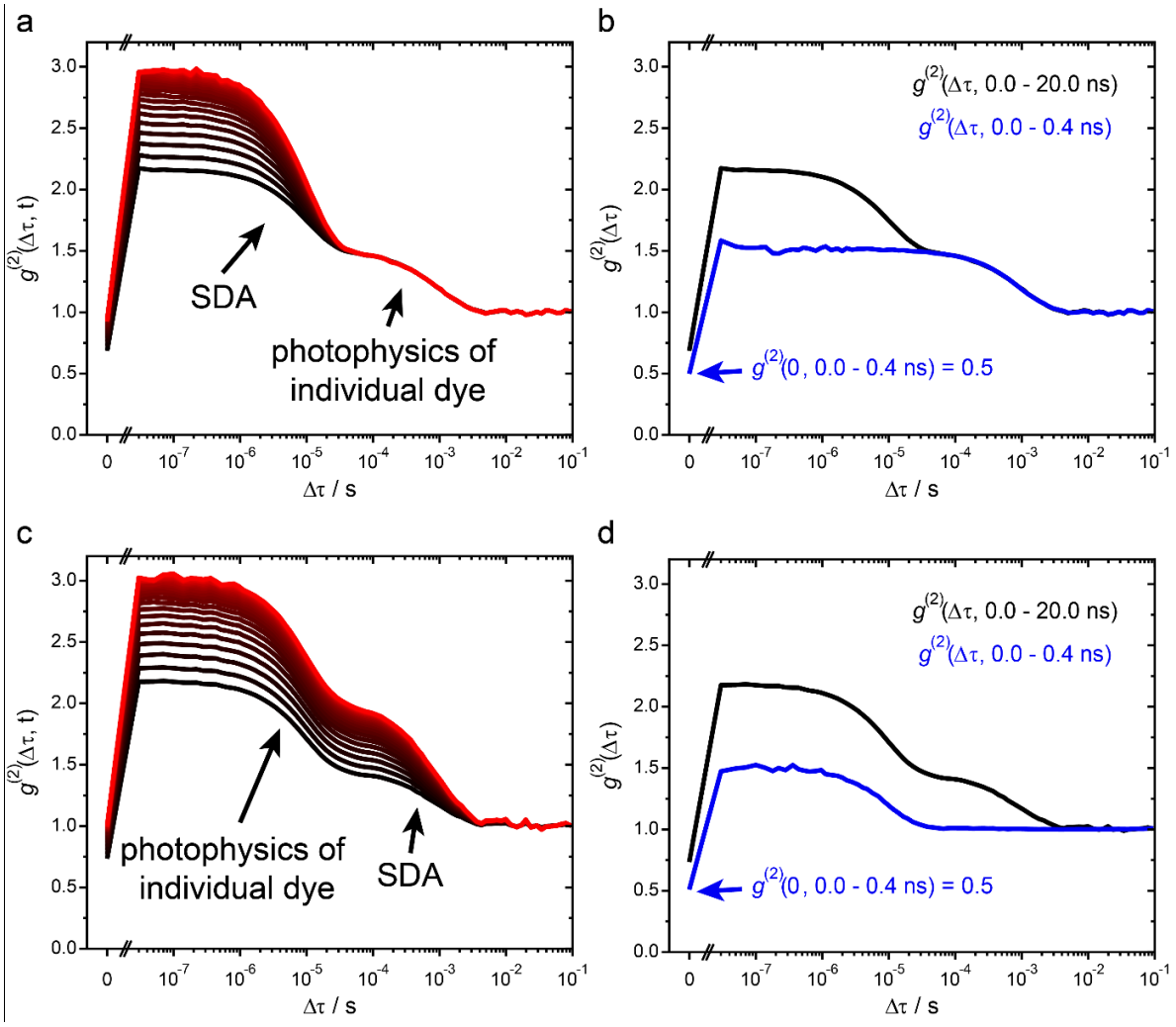

Figure S12. (a, c) Simulated intensity correlation of two collectively blinking dyes, which also show individual blinking. The color gradient marks the beginning of the microtime gate t used, which was shifted in steps of 200 ps. Black corresponds to an early (from $0\ ns$) beginning of the microtime gate and red to a late one (up to 5 ns). (b, d) Intensity correlation curves considering all photons (black) and only the photons detected within the first 400 ps after pulsed excitation (blue). Note that the bunching amplitude due to collective blinking is missing and that $g^{(2)}(0)$ yields the correct degree of photon antibunching.

The expected antibunching value for two dyes is 0.5. The simulation with faster collective blinking (SDA, Figure S12a) kinetics yields a degree of photon antibunching of $g^{(2)}(0) = 0.69$ and $N_c/N_\ell = 0.32$. The simulation with faster individual blinking (Figure S12c) yields a degree of photon antibunching of $g^{(2)}(0) = 0.73$ and $N_c/N_\ell = 0.34$. $g^{(2)}(0)$ overestimates the number of dyes because collective blinking is present, which raises the $g^{(2)}(0)$ value. N_c/N_ℓ underestimates the number of dyes because the lateral correlation bins are now the sum of the two bunching amplitudes but only the amplitude of the collective blinking is affecting the zero-lag-time correlation $g^{(2)}(0)$.

An easy approach to count the number of chromophores is the application of a small microtime gate right after the pulsed excitation. The quenching of the SDA is a time dependent process and becomes more likely as time progresses, which ultimately results in a quenched fluorescence intensity and shortened fluorescence lifetime. If there were only little time for SDA processes, both intensity levels would be equally bright if only photons right after the laser pulse excitation are considered. Within the first few hundred picoseconds no intensity fluctuations due to SDA are observed, resulting in an absence of bunching amplitude in the intensity correlation as depicted by the blue lines in Figure S12b,d. The remaining bunching amplitude results from the independent blinking process and therefore the number of chromophores can be reliably counted by $g^{(2)}(0)$ as demonstrated in Figure S12b,d. Choosing an early time gate is also useful if SSA has to be considered, which is also a time dependent process.[9] With an early microtime gate annihilation processes have most likely not occurred yet and no excitons are lost due to SSA nor SDA.

Table S4: Sequences for the modified DNA origami structure.

5‘ position	**Sequence**	**Comment**
0[286]	AAAACGAAAGAGGCTCATTATAC	
11[105]	ACACAACATACGAGGGATGTGGCTATTAATCGGCC	
9[567]	ATCATTTACATAAAAGTATCAAAATTATAAGAAACTTCAATA	
7[567]	CAGCTTTGAATACCAAGTTACAA	
5[455]	CATGCCAGTGAGCGCTAATATCCAATAATAAGAGC	
2[223]	CCGAACTTTAATAAAAGCAAAGCGGATT	
5[497]	TTGAGAATATCTTTCCTTATCACTCATCGAGAACA	
9[315]	CAGATATAGGCTTGAACAGACGTTAGTAAAGCCCAAAAATTT	
5[287]	GCGCAGCGACCAGCGATTATATATCATCGCCTGAT	
8[69]	TCGGTCATACCGGGGGTTTCTGC	

11[219]	GTGCCTGCTTTAAACAGGGAGAGAGTTTCAAAGCGAACCA	
10[457]	AAAAGATAGGGTTGAGTGT	
2[643]	GATAGTGCAACATGATATTTTTGAATGG	
0[347]	AGCGTATCATTCCACAGACCCGCCACAGTTGCAGCAAGCG	
9[483]	ATAATGAATCCTGAGATTACGAGCATGTGACAAAAACTTATT	
8[573]	AAATGCGTTATACAAATTCTTAC	
2[433]	AGGGACAAAATCTTCCAGCGCCAAAGAC	
7[63]	GCCCGCACAGGCGGCCTTTAGTG	
4[377]	CTATTTCGGAACGAGTGAGAATA	
0[698]	TTTTTCGGGAGCTAAACAGGTTGTTAGAATCAGAGTTTTT	
4[587]	CATCGGGAGAAATTCAAATATAT	
7[506]	AAATCAGCCAGTAATAACACTATTTTTGAAGCCTTAAATC	
7[170]	TTTTTATCCAATAAATCTCTACCCCGGTAAAACTAGCATG	
5[161]	GTATACAGGTAATGTGTAGGTAGTCAAATCACCAT	
4[396]	AACAGAGTGCCTGGGGTTTTGCTCACAGAAGGATTAGGAT	
3[350]	GTCACCAGTACAAGGTTGAGGCA	
5[581]	ACATCATTTAAATTGCGTAGAAACAGTACCTTTTA	
5[623]	ATACCCTTCGTGCCACGCTGAACCTTGCTGAACCT	
8[130]	GGGCGTGAAATATTAGCGCCATTCGC	
9[357]	TCTTATACTCAGAAAGGCTTTTGATGATATTGACACGCTATT	
11[345]	GAGAGCCTCAGAACCGCATTTTCTGTAACGATCTAAAGTT	
5[329]	TTCATTTTCTGCTAAACAACTGAACAACTAAAGGA	
8[489]	AAAACGGAATACCCAAAAGAACT	
0[202]	GACCGGAAGCAATTGCGGGAGAA	
3[182]	GCTAAATCGGTTTGACTATTATA	
3[392]	ATATTCACAAACAAATTCATATG	
6[69]	AAAAGTGTCAGCAACAATTGCAGGCGCT	
11[567]	ACCATCACCCAAATAAACAGTTCATTTGATTCGCC	
7[590]	AATCGTTGAGTAACATTGGAATTACCTAATTACATTTAAC	
11[93]	GCTCAAGTTGGGTAACGGGCGGAAAAATTTGTGAGAGATA	
0[305]	ACTACCTTTAAACGGGTAACAGGGAGACGGGCA	
4[270]	TCAACATCAGTTAAATAGCGAGAGTGAGACGACGATAAAA	
6[153]	TAAATCGGTTGGTGCACATCAAAAATAA	
10[163]	TCAGCTAACTCACATTAAT	
7[231]	TGCAACACTATCATAACCCTCGT	
4[438]	ACCAAATTACCAGGTCATAGCCCCGAGTTTTCATCGGCAT	
8[195]	TTAACAAGAGAATCGATGAACGG	
3[625]	AGACAACCTGAACAGTATTCGAC	
8[363]	TGAACAGCTTGATACCGATAGTT	
0[412]	TCACCGTCACCGGCGCAGTCTCT	
4[706]	TTTTTGTCCATCACGCAAATTCCGAGTAAAAGAGTCTTTTTT	

11[315]	ACAGCTGATTGCCCGTCGCTGCGCCCACACGTTGA	
8[424]	CGGAAGCACGCAAACTTATTAGCGTT	
0[431]	ATTCAAGGGGAAGGTAAATGTGGCAAATAAATC	
3[602]	TGATTATCAGATATACGTGGCAC	
4[545]	TGACCTAAATTTTTAAACCAAGT	
3[679]	GGTTGCTTTGACGAGCACGTTTTT	
6[573]	TGATTTAGAAAACTCAAGAGTCAATAGT	
11[441]	AAAAGAATAGCCCGATACATACGCAGTAAGCTATC	
8[634]	TACATAAATTCTGGGCACTAACAACT	
3[541]	CATAGTTAATTTGTAAATGTCGC	
11[147]	TGCCTAATGAGTGAGAAAAGCTCATATGTAGCTGA	
9[651]	AATAGCTGTCACACGCAACGGTACGCCAGCGCTTAATGTAGTA	
0[557]	TACCTAATATCAAAATCATTCAATATTACGTGA	
4[60]	TCAGAGGTGTGTCGGCCAGAATGAGTGCACTCTGTGGT	
3[476]	TTTTTTGTTTAATAAAGTAATTC	
8[382]	AAGTAAGAGCCGCCAGTACCAGGCGG	
3[79]	GTGGAACGACGGGCTCTCAACTT	
4[102]	CCAGCCAAACTTCTGATTGCCGTTTTGGGTAAAGTTAAAC	
3[121]	AATCAGTTAAAACGTGGGAGAAA	
3[224]	GCATCAAAAAGAAGTAAATTGGG	
7[212]	TTTCACGAGAATGACCATTTTCATTTGGTCAATAACCTGT	
8[678]	CCTACATACGTAGCGGCCAGCCATTGCAACAGGTTTTT	
5[539]	TTCGCTATTCGCAAGACAAAGTTAATTTCATCTTC	
7[17]	TTTTTATCCAGCGCAGTGTCACTGC	
8[298]	CATAGAATTTGCGGTTTGAAAGAGGA	
10[79]	GTATGTGAAATTGTTATCC	
7[273]	ACTACTTAGCCGGAACGAGGCGC	
11[387]	GGCGACACCACCCTCAGGTTGTACTGTACCGTTCCAGTAA	
6[447]	TTACCTCTTAGCAAATTTCAACCGATTG	
8[508]	GGTTTGCGCATTTTAACGCGAGGCGT	
10[415]	CCTCCGAAATCGGCAAAAT	
4[480]	TAAGCCAGAGAGCCAGAAGGAAACTCGATAGCCGAACAAA	
0[179]	GCCTTATACCCTGTAATACCAATTCTTGCGCTC	
9[147]	CATTCAACCCAAAATGTAGAACCCTCATGAATTAGTACAACC	
7[525]	TATGTGATAAATAAGGCGTTAAA	
0[454]	AGACGGGAGAATTGACGGAAATT	
11[681]	AAAGGGCGCTGGCAAGTATTGGC	
4[228]	GAGCTTAAGAGGTCCCAATTCTGCAATTCCATATAACAGT	
3[331]	TACCGGGATAGCAATGAATATAT	
4[335]	ATTGCGAATAATGTACAACGGAG	
2[265]	TATGCATTACAGAGGATGGTTTAATTTC	

4[564]	TTTAGAACGCGAATTACTAGAAAACTATAAACACCGGAAT	
11[597]	GAGGTAACGTTATTAATTTTAAAACAAATAATGGAAGGGT	
5[25]	TTTTTCCGGTGCAGCACCGATCCCTTACACTTGCC	
1[17]	TTTTTTGGTAATGGGTAACCATCCCACTTTTT	
8[531]	AACGAACCTCCCGACTTGCGGGA	
0[515]	CTGAAAACCTGTTTATCAAACATGTAACGTCAA	
8[592]	AAAATTTTTTAAAATGAGCAAAAGAA	
7[609]	ATTTGGCAAATCAACAGTTGAAA	
11[639]	CCGATAATAAAAGGGACTTAACACCGCGAACCACCAGCAG	
3[583]	GGAATCGGAACATTGCACGTTAA	
2[349]	TGTAGGGGATTTAGTAACACTGAGTTTC	
3[434]	AAAAGGGCGACAATTATTTATCC	
5[371]	ATCAGAGCCTTTAACGGGGTCTTAATGCCCCCTGC	
7[338]	GGAGCAGCCACCACCCTTCGCATAACGACAATGACAACAA	
3[56]	ATCAGCGGGGTCAGCTTTCAGAG	
0[473]	AAAAAAGGCAGCCTTTACAATCTTACCAGTTTG	
6[698]	TTTTTAACAATATTACCGTCGCTGGTAATATCCAGTTTTT	
8[88]	AGCCTCCCCAGGGTCCGGCAAACGCG	
6[405]	CAAGTGCTGAGTAAGAAAATAAATCCTC	
7[632]	GGAATAACAGAGATAGACATACAAACTTGAGGATTTAGAA	
0[76]	GACTTTCTCCGTGGCGCGGTTG	
2[97]	GCGAAAGACGCAAAGCCGCCACGGGAAC	
4[648]	GCATCGAGCCAGATATCTTTAGGACCTGAGGAAGGTTATC	
4[606]	ACAGTTTTTCAGATTTCAATTACCGTCGCAGAGGCGAATT	
7[548]	TAAGATCTGTAAATCGTTGTTAATTGTAAAGCCAACGCTC	
11[555]	CCCACATGTGAGTGAATAACTGATGCTTTTAACCTCCGGC	
9[399]	ATAAGAAGCCACCCAAACTTGAGCCATTATCAATACATCAGT	
11[189]	ACTGCCCGCTTTCCTGAAAAGCTATATTTTAAATA	
3[499]	TGTCCAAGTACCAGAAACCCCAG	
4[209]	AATGCTGTAGCTGAGAAAGGCCG	
7[357]	GTGTATTAAGAGGCTGAGACTCC	
8[237]	GCTTGACCATTAGATACATTTCG	
9[609]	GATGAATAAATCCTGTAGGTGAGGCGGTAGCGTAAGTCCTCA	
0[328]	TTGTCGTCTTTCTACGTAATGCC	
11[513]	CTCCAATTTAGGCAGAGACAATCAATCAAGAAAAATAATA	
3[560]	AAGACGCTGAGACCAGAAGGAGC	
7[42]	GCGCCTGAATGCCAACGGCCCAGCCTCCCGCGTGCCTGTTCTTCTTTTT	
0[370]	GCGTCATACATGCCCTCATAGTT	
11[303]	GTGAGTTAAAGGCCGCTGACACTCATGAAGGCACCAACCT	
3[373]	GGTCACGCCAGCACAGGAGTTAG	
4[51]	GGGTTACCTGCAGCCAGCGGTGTTTTT	

7[254]	TTACCAATAAGGCTTGCAGTGCGGAAGTTTAGACTGGATA	
8[466]	GGCATAAGCGTCTTCGAGGAAACGCA	
3[247]	CTTGAAAACACCCTAACGGCATA	
8[405]	GGTGCCGTCGAGAGGGTTGATAT	
10[331]	TCGTTCACCGCCTGGCCCT	
8[615]	GTTGAAACAAACATCAAGAAAAC	
6[531]	GACCGTCGAACGGGGAAGCTAATGCAGA	
6[363]	TGAAATTGTTTCAGGGAACTACAACGCC	
10[625]	AACACCCTAAAGGGAGCCC	
6[279]	CATGTCAGAGATTTGATGTGAATTACCT	
11[429]	CCCTTCATATAAAAGAACGTAGAGCCTTAAAGGTGAATTA	
11[651]	TTGACGGGGAAAGCTTCACCAGAAATGGCATCACT	
6[615]	GTCAGTCGTTTAACGAGATGGCAATTCA	
7[422]	AGCGCCACCACGGAATACGCCTCAGACCAGAGCCACCACC	
4[312]	ATTTGCCAAGCGGAACTGACCAACGAGTCAATCATAAGGG	
8[550]	CAGTAAGAACCTTGAGCCTGTTTAGT	
4[503]	AGCAAGCCGTTTAAGAATTGAGT	
2[601]	TCAATAATAAAGTGTATCATCATATTCC	
9[21]	TTTTTGCGTCCGTGCCTGCATCAGACGTTTTT	
11[483]	GAACAAGAGTCCACCAATTTTTTAGTTGTCGTAGG	
10[499]	CTATATTAAAGAACGTGGA	
4[186]	GAGACAAAGATTATCAGGTCATTGACGAGAGATCTACAAA	
9[63]	TTCACCTAGCGTGGCGGGTGAAGGGATACCAGTGCATAAAAA	
11[609]	AGCACTAAATCGGATCGTATTTAGACTTATATCTG	
4[293]	AAATTGTGTCGAGAATACCACAT	
3[667]	GGCGCCCCGCCGAATCCTGAGAAGTGAGGCCGATTAAAGG	
3[205]	GTCAGAATCAGGCAGGATTCGCG	
0[622]	AAGATAAAACAGTTGGATTATAC	
6[111]	TCAGGTGAAATTTCTACGGAAACAATCG	
10[205]	AGCAGTCGGGAAACCTGTC	
6[489]	AATCATAATAACCCGGCGTCAAAAATGA	
0[496]	TCCCATCCTAATGAGAATAACAT	
0[221]	CGAGCACAGACTTCAAATACCTCAAAAGCTGCA	
9[231]	TTAGTGTGAATCCCTCTAATAAAACGAAAGAACGATGAATTA	
4[629]	CAAATATCAAACCAGATGAATAT	
0[664]	GATTTTAGACAGGCATTAAAAATA	
10[667]	AGACGGCGAACGTGGCGAG	
0[599]	TTCTGGAATAATCCTGATTTTGCCCGGCCGTAA	
3[23]	TTTGCAACCAGCTTACGGCGGTGGTGAGGTTTCAGTTGAGGATCCTTTTT	
8[340]	GCGCCCGCACCCTCTCGAGGTGAATT	
7[674]	GCCTTACGCTGCGCGTAAAATTATTTTTTGACGCTCAATC	

7[86]	ATGAATCCCAGTCACGATCGAACGTGCCGGCCAGAGCACA	
5[245]	CGCCTGACGGTAGAAAGATTCTAATGCAGATACAT	
8[657]	GTATTAGAGCCGTCAATAGATAA	
3[308]	CTAAAGACTTTTAGGAACCCATG	
2[702]	TTTTTTATAACGTGCTTTCCTCTTTATAACAGTACTAT	
4[671]	TACTTCTTTGATAAAAATCTAAA	
2[391]	ATTAAAATAAGTGCGACGATTGGCCTTG	
9[189]	GAGCAAGGTGGCATTTACTCCAACAGGTTCTTTACGTCAACA	
4[167]	CAATATGATATTGATGGGCGCAT	
7[147]	GCTAATGCCGGAGAGGGTAGCTA	
7[464]	AAGCACAGAGCCTAATTATTGTTAGCGATTAAGACTCCTT	
8[172]	TAATCGTAGCATTACCTGAGAGTCTG	
0[580]	TAGAACCTACCAGTCTGAGAGAC	
4[354]	GAAAGTTCAACAATCAGCTTGCTTAGCTTTAATTGTATCG	
8[46]	CAGCATCAACCGCACGGCGGGCCGTT	
2[181]	TTATGGCCTGAGCACCTCAGAGCATAAA	
3[644]	CTATTAGTCTTTCGCCGCTACAG	
8[111]	CTTTTTTTCGTCTCGTCGCTGGC	
11[231]	TTAATGAATCGGCCATTCATTCCAATACGCATAGT	
3[518]	AACAACATGTTCATCCTTGAAAA	
5[77]	AACGTTGTAGAAACAGCGGATAGTTGGGCGGTTGT	
10[706]	TTTTTAGGAGCGGGCGCTAGGAAGGGAAGAAAGCGAATTTTT	
9[441]	TGCCATACATAAAGATTAACTGAACACCAACAGCCGGAATAG	
7[189]	GGCTAAAGTACGGTGTCTGGAAG	
6[237]	AAGAGATTCATTTTGTTTAAGAGGAAGC	
5[203]	TGTAAATCATGCTCCTTTTGATAATTGCTGAATAT	
7[315]	AATCCAAAAAAAAAGGCTCCAAAA	
10[583]	TGGCAAGTTTTTTGGGGTC	
2[559]	GAATTATCCAATAACGATAGCTTAGATT	
11[364]	GTCCACGCGCCACCTCACCGTTGAAACA	
11[471]	TGTTCCAACGCTAACGAACAAGTCAGCAGGGAAGCGCATT	
4[522]	ACCGCATTCCAACGGTATTCTAAGCGAGATATAGAAGGCT	
7[380]	TCAAGCAGAACCACCACTCACTCAGGTAGCCCGGAATAGG	
8[447]	ATTCTTTTCATAATCAAAATCAC	
6[321]	AAATCCCCGAAACAATTCATGAGGAAGT	
10[541]	CATTCTATCAGGGCGATGG	
10[373]	TACCTGGTTTGCCCCAGCA	
5[413]	AGAGTTTATACCAGTAGCACCTGAAACCATCGATA	
9[105]	GTCCGTCCTGCAAGATCGTCGGATTCTCTTCGCATTGGACGA	
11[63]	ATAGCTGTTTCCTGGAACGTCCATAACGCCGTAAA	
11[177]	TGCGTACTAATAGTAGTTGAAATGCATATTTCAACGCAAG	

8[702]	TTTTTAAAAACGCTCATGGAAATA	
7[441]	TTGAAGCCCTTTTTAAGAAAAGT	
11[525]	AGGGCGAAAAACCGATTTAACGTAGGGCAAATACC	
2[475]	AAATAGGTAATTTACAAATAAGAAACGA	
9[525]	TTTAGCAAACGCCACAATATAACTATATTCCCTTATAAATGG	
7[399]	TATTGCCTTTAGCGTCAGACTGT	
0[389]	GAATTGTAGCCAGAATGGATCAGAGCAAATCCT	
2[307]	TTCCATTGACCCAAAGAGGCTTTGAGGA	
7[651]	TAAGTAGAAGAACTCAAACTATCG	
2[517]	ACGCGTCGGCTGTAAGACGACGACAATA	
7[483]	GTTTACCGCGCCCAATAGCAAGC	
2[55]	TTCGCCATAAACTCTGGAGGTGTCCAGC	
10[48]	GCAGCACTTTGCTCTGAGCCGGGTCACTGTTGCCCTGCGGCTTTTT	
6[657]	TGCCTGAACAGCAAATGAATGCGCGAACT	
3[163]	TAAAGAGGCAAAATATTTTATAA	
0[538]	TTAGGTTGGGTTATAGATAAGTC	
4[419]	GCAGCACCGTAAGTGCCCGTATA	
8[214]	CAAATGGTTCAGAAGAACGAGTAGAT	
3[415]	GTTTATGTCACATGGGAATCCAC	
0[641]	CCGAACCCCCTAAAACATCGACCAGTTTAGAGC	
8[321]	CCGAACGGTGTACAGACCAGGCG	
3[457]	CAATCCAAAATACTGAACAGTAG	
6[195]	TGCAACTCAAAAGGCCGTACCAAAAACA	
0[95]	CCGGAAGACGTACAGCGCCGCGATTACAATTCC	
11[399]	GTTTGATGGTGGTTCAGAACCCCGCCTCACAGAAT	
11[25]	TTTTTCCGGGTACCGAGCTCGAATTCGTAATCTGGTCA	
0[53]	CGGTAGTACTCAATCCGCTGCTGGTCATGGTC	
8[256]	AAAATTCCATTCAGGCTTTTGCAAAAGAAGTCA	
3[266]	AACTTTAATCATGGGTAGCAACGGCTACGACAGCAACTAAAA	
10[247]	AATAACGCGCGGGGAGAGGCGGTT	
0[251]	TGGGAAGAAAAATCTACGTGCGTTTTAATT	
0[263]	CAGTCTTGATTTTAAGAAC	
8[286]	GACCTTCATTTTGCCAGAGGGGGTAATAGT	
7[296]	AGACGTCGTCACCCTCAGACCTGCTC	
10[293]	ACCGGATGTTTTTCTTTTCACCA	ATTO 647N, only used for independent blinking
10[286]	ATTCATTAGAGTAATCTTGACGCTGGCT	
4[461]	AAGAAACAATGACCGGAAACGTC	biotin labeled
4[83]	GTACATCGACATCGTTAACGGCA	biotin labeled
5[665]	ATACCACCATCAGTGAGGCCAAACCGTTGTAGCAA	biotin labeled
4[251]	AACGCCAAAAGGCGGATGGCTTA	biotin labeled

5[119]	CATAATATTCCGTAATGGGATCCGTGCATCTGCCA	external labeling
3[98]	GGATAACCTCACAATTTTTGTTA	external labeling
4[125]	GTTTGAGGGGACCTCATTTGCCG	external labeling
4[144]	CGTAAAGGTCACGAAACCAGGCAATAGCACCGCTTCTGGT	external labeling
0[137]	CATCAGCGTCTGGCCTTCCACAGGAACCTGGGG	external labeling
10[121]	GGGCCGGAAGCATAAAGTG	external labeling
11[135]	TAAAGGATTGTATAAGCGCACAAACGACATTAAATGTGAG	external labeling
7[128]	TTCCGAATTGTAAACGTGTCGCCAGCATCGGTGCGGGCCT	external labeling
3[140]	CAATAGGAACGCAAATTAAGCAA	external labeling
7[105]	GAAAGATCGCACTCCAGCCAGCT	external labeling
0[160]	GATAAAAATTTTTAGCCAGCTTT	external labeling
8[153]	TCAGGCTGCGCAACTGTTGGGAA	external labeling
0[118]	CGAGTAACAACCGTTTACCAGTC	external labeling
2[139]	TTCGCGGATTGATTGCTCATTTTTTAAC	external labeling
10[279]	ACCCAAATGGCAAAAGAATACTCGGAACAGAATCC	5' ATTO 647N, only used for collective blinking
10[265]	AACAAAGCTGCTGTAACAACAAGGACGT	5' ATTO 647N
10[272]	TCAACGTTGCGTATTGGGCGCCAGGGTG	5' ATTO 700, only used for collective blinking

REFERENCES

1. Nickels, P. C.; Wünsch, B.; Holzmeister, P.; Bae, W.; Kneer, L. M.; Grohmann, D.; Tinnefeld, P.; Liedl, T. Molecular Force Spectroscopy with a DNA Origami-Based Nanoscopic Force Clamp. *Science* **2016**, *354*, 305–307.
2. Derr, N. D.; Goodman, B. S.; Jungmann, R.; Leschziner, A. E.; Shih, W. M.; Reck-Peterson, S. L. Tug-of-War in Motor Protein Ensembles Revealed with a Programmable DNA Origami Scaffold. *Science* **2012**, *338*, 662–665.
3. Laurence, T. A.; Fore, S.; Huser, T. Fast, Flexible Algorithm for Calculating Photon Correlations. *Opt. Lett.* **2006**, *31*, 829–831.
4. Schröder, T.; Scheible, M. B.; Steiner, F.; Vogelsang, J.; Tinnefeld, P. Interchromophoric Interactions Determine the Maximum Brightness Density in DNA Origami Structures. *Nano Lett.* **2019**, *19*, 1275–1281.
5. Zumbusch; Fleury; Brown; Bernard; Orrit. Probing Individual Two-Level Systems in a Polymer by Correlation of Single Molecule Fluorescence. *Phys. Rev. Lett.* **1993**, *70*, 3584–3587.
6. Orrit, M. Photon Statistics in Single Molecule Experiments. *Single Mol.* **2002**, *3*, 255–265.
7. Lamb, D. C.; Schenk, A.; Röcker, C.; Nienhaus, G. U. Determining Chemical Rate Coefficients Using Time-Gated Fluorescence Correlation Spectroscopy. *J. Phys. Org. Chem.* **2000**, *13*, 654–658.
8. Yu, J.; Lammi, R.; Gesquiere, A. J.; Barbara, P. F. Singlet-Triplet and Triplet-Triplet Interactions in Conjugated Polymer Single Molecules. *J. Phys. Chem. B* **2005**, *109*, 10025–10034.

9. Hedley, G. J.; Schröder, T.; Steiner, F.; Eder, T.; Hofmann, F. J.; Bange, S.; Laux, D.; Höger, S.; Tinnefeld, P.; Lupton, J. M.; Vogelsang, J. Picosecond Time-Resolved Photon Antibunching Measures Nanoscale Exciton Motion and the True Number of Chromophores. *Nat. Commun.* **2021**, *12*, 1327.